Chemical preservation of tail feathers from Anchiornis huxleyi , a theropod dinosaur from the Tiaojishan Formation (Upper Jurassic, China)

Aude Cincotta, Thanh Thuy Nguyen Tu, Julien Colaux, Guy Terwagne, Sylvie Derenne, Pascal Godefroit, Robert Carleer, Christelle Anquetil, Johan Yans

Chemical preservation of tail feathers from *Anchiornis huxleyi*, a theropod dinosaur from the Tiaojishan Formation (Upper Jurassic, China)

Aude Cincotta[1], Thanh Thuy Nguyen Tu[2], Julien L. Colaux[3], Guy Terwagne[4], Sylvie Derenne[2], Pascal Godefroit[5], Robert Carleer[6], Christelle Anquetil[2], and Johan Yans[7]

[1] School of Biological, Earth and Environmental Sciences, University College Cork, Distillery Fields, North Mall, Cork, Ireland T23 N73K; email: aude.cincotta@ucc.ie

[2] Sorbonne Université, CNRS, EPHE, PSL, UMR 7619 Metis, 4 place Jussieu, 75252 Paris cedex 05, France

[3] Synthesis, Irradiation and Analysis of Materials (SIAM), Department of Physics, University of Namur, 61 rue de Bruxelles, 5000 Namur, Belgium.

[4] Laboratoire d'Analyses par Réactions Nucléaires (LARN), Department of Physics, University of Namur, 61 rue de Bruxelles, 5000 Namur, Belgium.

[5] Operational Directorate 'Earth and History of Life', Royal Belgian Institute of Natural Sciences, 29 rue Vautier, 1000 Brussels, Belgium.

[6]Applied and Analytical Chemistry, Institute for Material Research, University of Hasselt, Campus Diepenbeek, Agoralaan Building D, 3590 Diepenbeek.

[7]Institute of Life, Earth and Environment, University of Namur, 61 rue de Bruxelles, 5000 Namur, Belgium.

Abstract: A panel of geochemical techniques is used here to investigate the taphonomy of fossil feathers preserved in association with the skeleton of the Jurassic theropod *Anchiornis huxleyi*. Extant feathers were analysed in parallel to test whether the soft tissues morphologically preserved in the fossil also exhibit a high degree of chemical preservation. Scanning electron microscopy (SEM) and energy dispersive spectroscopy (EDS) indicate that clays and iron oxide pseudomorphs occur in the surrounding sediment and also reveal the preservation of melanosome-like microbodies in the fossil. Carbon gradient along a depth profile and co-occurrence of carbon and sulphur are shown in the fossil by elastic backscattering (EBS) and particle-induced X-ray emission (PIXE), which are promising techniques for the elemental analysis of fossil soft tissues. The molecular composition of modern and fossil soft tissues was assessed from micro-Attenuated Total Reflectance Fourier Transform Infrared spectroscopy (micro-ATR FTIR), solid-state ^{13}C nuclear magnetic resonance (^{13}C CP-MAS NMR) and pyrolysis- gas chromatography-mass spectrometry in the presence of TMAH (TMAH-Py-GC-MS). Results indicate that the proteinaceous material that comprises the modern feathers is not present in the fossil feathers. The latter and the embedding sediment exhibit a highly aliphatic character. However, substantial differences exist between these samples, revealing that the organic matter of the fossil feathers is, at least partially, derived from original constituents of the feathers. Our results suggest that, despite the morphological preservation of *Anchiornis* feathers, original proteins, i.e. keratin, were probably not preserved in the 160-Ma-old feathers.

Key words: *Anchiornis*; fossil feathers; taphonomy; soft tissue preservation; dinosaur.

INTRODUCTION

Preservation of soft-bodied animals – with non-mineralized tissues – is relatively rare, when considering the whole geological record. Soft parts of organisms are usually lost during the diverse degradation processes occurring during fossilization. Their constitutive labile organic compounds are usually too fragile to be preserved, compared to the 'hard' – biomineralized – parts, which are generally better preserved. However, some important fossil-bearing sites yield not only exquisitely preserved skeletons but also remains of soft tissues, such as skin, scales, hair or feathers (e.g. Allison and Briggs 1993; Zhu *et al*. 2005; Pan *et al*. 2013). Feathers, the epidermal appendages that form the external covering of modern birds, have been discovered preserved in close association with fossils of theropod dinosaurs in Konservat-Lagerstätten – localities that are characterized by the unusual quality of the fossils – from the Upper Jurassic and Lower Cretaceous of China (Hu *et al*. 2009; Xu *et al*. 2012; Xu *et al*. 1999; Xu *et al*. 2009; Chu *et al*. 2016; Godefroit *et al*. 2013) and Germany (Rauhut *et al*. 2012). During the last twenty years, Liaoning Province, in north-eastern China, has yielded well-preserved vertebrate fossils with soft parts (e.g. Benton *et al*. 2008; Kellner *et al*. 2010; Li *et al*. 2012). The most striking discoveries were exquisitely well-preserved feathered theropod dinosaurs, evidencing their relationship with modern birds. Since the discovery of the Early Cretaceous *Sinosauropteryx prima* in 1996 (Ji and Ji 1996), many other feathered specimens have been found (Hu *et al*. 2009; Li *et al*. 2012; Xu *et al*. 2012; Xu *et al*. 2015). In the same way, the discovery of one of the most primitive birds, *Archaeopteryx lithographica*, associated with well-preserved feathers, constitutes a gigantic step in the comprehension of bird – and feather – evolution (Christiansen and Bonde 2004). Interestingly, elongate filaments interpreted as primitive feathers were observed in ornithischian – non-theropod – dinosaurs (Mayr *et al*. 2002; Zheng *et al*. 2009). Recently, both 'feather-like' structures and scales were discovered together with remains of

the middle Jurassic neornithischian *Kulindadromeus zabaikalicus* collected in volcanoclastic deposits from Siberia (Godefroit *et al*. 2014; Cincotta *et al*. 2019; Godefroit *et al*. 2020). Recently, a small theropod dinosaur, the scansoriopterygid *Ambopteryx longibrachium* (Wang et al. 2019) from the Upper Jurassic of China, was described with membranous wings instead of feathered ones. This wing configuration was probably lost during evolution in favour of the feathered wing configuration that occurs in modern birds.

In a recent study, Zhao *et al*. (2020) observed the structure of experimentally matured feathers and reported the fusion of barbules in the matured feathers. This result has implications in terms of feather taphonomy and evolution, for the absence of barbules in fossil feathers could be due to their fusion during diagenesis instead of their true absence in the specimen. This is unfortunate that no chemical analyses have been performed to better understand how maturation affects the preservation of biomolecules in feathers.

Fossil feathers show a wide range of preservation degrees (e.g. Schweitzer 2011; Xing *et al*. 2016). The study of these diversely preserved structures is crucial for a better understanding of the taphonomic processes leading to their preservation. In most cases, feathers and other types of preserved soft-tissues were deposited in calm, low-energy environments (e.g. Kellner and de Almeida Campos 2002). They are found in diverse environmental settings such as shallow-marine (e.g. Martill and Heimhofer 2007; Barthel 1964; Heimhofer and Martill 2007), lacustrine (e.g. Harms 2002; Sullivan *et al*. 2014; Zhou and Wang 2010), or terrestrial (Manning *et al*. 2013). Different modes of preservation occur for ancient soft tissues: carbonaceous films (e.g. Li *et al*. 2010; Lindgren *et al*. 2015), phosphate (Allison and Briggs 1993; Briggs *et al*. 1993), pyrite (Briggs *et al*. 1991; Farrell *et al*. 2013; Leng and Yang 2003), clay

minerals (Gabbott *et al*. 2001; Martin *et al*. 2004), aluminosilicates (Butterfield *et al.* 2007), or a combination of these (Wilby *et al*. 1996).

Feathers are epidermal appendages mainly composed of keratin (Lucas & Stettenheim 1972), which is present as two secondary structures, alpha-helixes and beta-sheets, corresponding to alpha- and beta-keratin, respectively (e.g. Fraser and MacRae 2012). Alpha-keratin plays a hydrophobic role in avoiding water loss, whereas beta-keratin increases skin hardness (Fraser and Parry 1996; Gregg and Rogers 1986). According to Lucas and Stettenheim (1972), the amino acid content of keratin in modern bird feathers is rather homogenous in identical parts of a feather (e.g. in rachis of feathers belonging to the same species), although it varies from one species to another. Nonetheless, feather keratin always comprises high amounts of serine, glycine, proline, and lower quantities of valine, leucine, alanine and cysteine (Arai *et al*. 1983, 1986; Gregg & Rogers 1986; Murphy *et al*. 1990; O'Donnell and Inglis 1974; Saravanan and Dhurai 2012a; Staroń *et al*. 2011).

The potential of keratin to resist diagenetic processes is still poorly known. Saitta *et al*. (2017) performed decay and maturation experiments of various keratinous structures, whose conclusions suggest that feather keratin would not survive diagenesis. Although the ultrastructure of feather keratin, i.e. fibrils, can be preserved (e.g. Lindgren *et al*. 2015), there is no direct evidence for the preservation of its proteinaceous compounds. Several immunohistological studies have suggested that keratin could be preserved (Schweitzer *et al*. 1999; Moyer *et al*. 2016; Pan *et al*. 2016), although this method remains highly controversial. By contrast, melanin – the natural pigment present in a variety of soft tissues including hair, skin and feathers – is considered to be more resistant to degradation and fossilization processes. Melanin has been unequivocally identified in various types of fossil tissues, such as fish eyes

(Lindgren *et al*. 2012), bird feathers (Colleary *et al*. 2015), non-avian dinosaur feathers (Lindgren *et al*. 2015), mammal hair (Colleary *et al*. 2015), or frog skin (McNamara *et al*. 2016).

Here, we investigate the ultrastructure and chemical composition of fossil feathers of a theropod dinosaur, *Anchiornis huxleyi* (YFGP-T5199), collected from Upper Jurassic deposits of the Tiaojishan Formation (Liaoning Province, China). Previous study of the same specimen focused on the identification of pigment remains (eumelanin), and evidenced the preservation of melanosomes in the feathers (Lindgren *et al*. 2015). We report new and complementary geochemical information about the preservation of macromolecular compounds in the fossil feathers using a range of analytical tools. The surrounding sediment and modern feathers were analysed in parallel to ascribe pristine constituents.

Scanning electron microscopy (SEM) and energy dispersive X-ray spectroscopy (EDS) were used to identify and characterize the elemental composition of preserved pigment organelles and the sedimentary matrix. X-ray diffraction (XRD) was used to analyse the mineralogical composition of the samples in an attempt to understand the role of sediment mineralogy in the preservation of soft tissues. Ion beam analysis (IBA), is recognised as a promising archaeometric tool (Jeynes and Colaux 2016) and has recently been successfully applied to human bone analyses (Beck 2014). In this work, Particle-Induced X-ray Emission (PIXE) and Elastic Backscattering Spectrometry (EBS) were used for the first time on fossil soft tissues to get insights into the heavy (PIXE) and light (EBS) in-depth elemental composition of the samples and demonstrate the co-occurrence of sulphur and carbon. This approach is innovative in the study of organic materials. Organic geochemistry techniques, micro-Attenuated Total Reflectance Fourier Transform Infrared Spectroscopy (micro-ATR FTIR), ^{13}C-Nuclear Magnetic Resonance (NMR), Pyrolysis Gas Chromatography-Mass Spectrometry in the presence of TMAH

(TMAH-Py-GC-MS), were applied to characterize the functional groups and other biomolecular components present in the studied samples. To our knowledge, the detailed chemical characterization by ^{13}C NMR and Py-GC-MS of fossil feathers from a non-avian dinosaur has not been done elsewhere.

MATERIAL AND METHODS

Specimen information

The studied specimen, *Anchiornis huxleyi* (YFGP- T5199) (Fig.1), is a basal Avialan (the description of the specimen is available in the Supplementary Information of Lindgren *et al*. 2015: pp. 18-23) that was collected from the Tiaojishan Formation in the Yaolugou locality (Liaoning Province, China), and belongs to the Yizhou Fossil and Geology Park in Liaoning. The Tiaojishan Formation consists of hundreds of meters of alternating sedimentary and volcanic beds (Liu *et al*. 2012; Yang *et al*. 2006; Yuan *et al*. 2005). Absolute dating on a laterally equivalent formation – the Lanqi Formation – indicates an age ranging between 165.0 ± 1.2 Ma and 153.0 ± 2.0 Ma (Chang *et al*. 2009; Zhang *et al*. 2008), which spans the Callovian-Kimmeridgian interval (Middle-Late Jurassic; Gradstein *et al*. 2012). YFGP-T5199 is embedded in thinly laminated carbonate sediments, corresponding to alternation of very thin marl and thicker clay laminae. These sediments were deposited in the context of a lake affected by episodic volcanic eruptions (Nan *et al*. 2012). Recent U-Pb radiochronological analyses on zircons from the Jianchang locality indicate that the Yanliao Biota, that includes *Anchiornis* as well as pterosaurs and

eutherian mammals, is Oxfordian in age (Chu *et al*. 2016). The plumage of the specimen studied herein is morphologically preserved as dark brown residues around the skeleton, especially around the tail and the forelimbs, and on the skull.

Sample description

The studied samples consist of fossil feather fragments dissected from the posterior end of the tail (Fig. 1, the dark area in the white box, top right) of YFGP- T5199, as well as fragments of the host sediment (Fig. 1, the light area in the white box). To test for possible chemical contamination of the fossil feathers by sediment, the sediment samples were analysed using the same methodology as for the fossil feathers. Two types of sediment samples were studied: (1) 'host' sediment directly in contact with the feathers from the tail (light area in white box on Fig. 1); and (2) 'remote' sediment located > 100 mm from the fossil on the same slab (yellow box bottom left on Fig. 1).

Sample preparation

Two modern brown wing feathers of *Buteo buteo* (buzzard, Aves: Accipitriformes; RBINS collection number: A4011A01; Supplementary Fig. 1) were analysed for comparative purposes. Different parts of the feathers, rachis and barbs, were analysed with IBA. The modern feathers come from a specimen that died naturally and was stored at -18°C at the Royal Belgian Institute of Natural Sciences prior to analysis.

Two types of samples were collected on the fossil specimen: millimetre-sized samples for SEM and EDS, as well as centimetre-sized samples for the other analytical approaches. We took 12 millimetre-sized samples (Fig. 1) from different regions of the body of YFGP-T5199 with a sterile scalpel. The

samples were mounted on double-sided carbon tape and sputter-coated with gold (Baltec SCD 050). Centimetre-sized fragments of approximately 5 mm² and 2 mm thick, from fossil feathers (white box in Fig. 1) and sediment (yellow box in Fig. 1) were dissected with a sterile scalpel. Samples were cleaned with distilled water without any additional preparation prior to analysis.

Several points were analysed with IBA and micro-ATR FTIR on two centimetre-sized fragments containing both fossil feathers and their 'host' sediment, and one fragment of 'remote' sediment (Supplementary Figs. 1B and 2). Other centimetric samples from the same region were collected for NMR and Py-GC-MS (white and yellow boxes on Fig. 1). These samples were crushed and lipids were extracted in order to (1) eliminate potential contaminants related to sample manipulation; and (2) concentrate macromolecular organic matter which mainly corresponds to proteins in modern feathers. Samples were ground to a fine homogeneous powder in an agate mortar. Lipid extraction involved three successive ultrasonications (ten minutes) in 15 ml of dichloromethane/methanol (2:1, v/v), at room temperature and centrifugation at 3500 rpm (ten minutes). The supernatant was removed and the pellet was dried under nitrogen and stored in the dark at 5 °C prior to analysis.

Analytical methods

Samples were imaged under low vacuum with an environmental QUANTA 200 (FEI) scanning electron microscope (at an acceleration voltage ranging from 20 to 30 kV and working distances of 8 to 15 mm). Subsequent semi-quantitative EDS analyses (single point and mapping) were performed using either an environmental QUANTA 200 (acceleration voltage of 30 kV and working distance of 10 mm) or a field-emission JEOL 7500F (acceleration voltage of 15 kV and a working distance of 8 mm).

194 XRD analyses were carried out on both bulk rock and clay mineral with a Philips diffractometer using
195 Cu K_α radiation. A tube voltage of 40 kV and a tube current of 30 mA were used. The goniometer
196 scanned from 3 to 70 degrees 2θ for the bulk rock and from 3 to 30 degrees 2θ for clay minerals. The
197 clay minerals (< 2 µm fraction) were isolated by successive centrifuging after decarbonatation of the
198 crushed rock with HCl 1N. The preparation was mounted on glass slides and treated according to the
199 three following protocols: (1) natural (air-dried); (2) ethylene-glycol solvation; and (3) heated at 490 $^{\circ}$C
200 for two hours. Clay minerals were identified according to the position of the (001), or (0001), series of
201 basal reflections on the X-ray diffractograms.

202 Elastic Backscattering Spectrometry (EBS) and Particle-Induced X-ray Emission (PIXE) measurements
203 were performed using a 3 MeV proton (^{1}H) beam from the Tandetron linear accelerator ALTAÏS
204 (University of Namur). PIXE is highly sensitive to Na to U elements whereas EBS signals are enhanced
205 for light elements (e.g. C, N and O) due to strong non-Rutherford cross-sections. These two integrative
206 methods, together, can identify almost all elements of the periodic table. The beam spot size was
207 reduced to 0.5 mm in diameter to minimize topographic effects. Backscattered particles were detected
208 using two detectors mounted at scattering angles of 170° and 165°, whereas the emitted X-rays were
209 collected with an Ultra-LEGe (Ultra Low Energy Germanium) detector mounted at 135°. Angles are
210 given relative to the incident beam direction. A selective filter (6 µm of Al) was mounted in front of the
211 Ultra-LEGe detector to lower the strong Si signal and therefore enhance the rather weak S signal
212 observed in the fossil feathers. The modern brown feathers were analysed at two different locations
213 (barb and rachis; Supplementary Figs. 1 and 2).Two locations were analysed in the fossil feathers. The
214 'host' sediment was analyzed at three different locations (at 1.7, 3.2, and 4.8 mm away from the fossil)
215 and the 'remote' sediment at one location (Supplementary Fig.2). All the samples were analysed using

the same experimental settings. A certified reference material (BCR-126A lead glass from NIST) was analysed to (1) calibrate the detectors (both EBS and PIXE); and (2) estimate the accuracy of the PIXE measurements. The EBS spectra were analysed with DataFurnace software (Jeynes *et al*. 2003) together with the cross-sections generated by SigmaCalc (Gurbich 2016) to derive the depth profiles of the major elements (see Supplementary Fig. 4 for carbon). The integral of C, O and Si depth profiles (integration limits set to 0 – 25 000 TFU[1], or 0 – 3 µm considering a density of 2.65 g/cm³) yields the C, O and Si equivalent thicknesses given in TFU (details on the global uncertainty calculations can be found in Supplementary Table 1). The PIXE spectra were manipulated with GUPIX software (Campbell *et al*. 2010). The matrix composition to be used in GUPIX was determined by integrating the depth profiles of the main components observed by EBS (i.e. C, O and Si) on a given interval (0 – 100 000 TFU).

Micro-Attenuated Total Reflectance Fourier Transform Infrared spectroscopy (micro-ATR FTIR) was performed on modern and fossil feathers using a Bruker Vertex 70 FTIR spectrometer (University of Hasselt, Belgium) equipped with a Hyperion 2000 microscope and MCT detector. The infrared spectra were collected in the mid-IR range, from 4000 to 600 cm^{-1}, and 32 scans were acquired in Attenuated Total Reflectance (ATR) mode (Ge –ATR crystal) with a resolution of 4 cm^{-1}. FTIR spectroscopy was used on a modern buzzard feather (dark regions), one sample of fossil feather from the tail of *A. huxleyi* and the surrounding sediment, to identify the presence or absence of functional groups in their molecular composition.

^{13}C Nuclear Magnetic Resonance is a spectroscopic method that documents the chemical environment of carbon in organic compounds. Solid state ^{13}C NMR spectra of the lipid-free samples were obtained at

125 MHz (Bruker Avance 500 spectrometer) using a 4 mm zirconium rotor, with a cross-polarization (CP) sequence and magic angle spinning (MAS) at 14 kHz. CP-MAS ^{13}C NMR spectra were acquired with contact time of 1 ms and recycle time of 1s (fossil and sediment) or 3s (modern feathers). The use of a single contact time does not allow precise quantification of the identified chemical functional groups. Each spectrum was the result of 6 000 (modern samples) to 400 000 (sediments) scans.

Curie point Pyrolysis-Gas Chromatography- Mass Spectrometry (Py-GC-MS) gives insight into the molecular composition of organic macromolecular materials through their thermal degradation into molecular building blocks that can be separated by gas chromatography (GC) and further identified by mass spectrometry (MS). Tetramethylammonium hydroxide (TMAH) was used to enhance the thermal breakdown of macromolecules and induce *in situ* methylation of pyrolysis products, which, in turn, enhance their detection and identification in GC-MS. The samples were mixed with an excess of TMAH (25 wt % in methanol) in a 1:1 (wt/wt) ratio before loading in ferromagnetic tubes with Curie temperature of 650 °C. Two mg were used for the modern samples, 6 mg for the fossil feathers, and 16 mg for the sediment. Curie point pyrolysis was carried out with a Pilodist Curie flash pyrolyser. Samples were heated at their Curie temperature for 10 s under a He flow of 1 ml/min. The instrument was coupled directly to a GC-MS system. The pyrolysis products were separated using a Trace Thermo gas chromatograph equipped with a Rxi5SilMS column (30 m × 0.25 mm i. d., 0.5 µm film thickness). Helium was used as carrier gas at constant pressure of 15 psi. The injector temperature was 280 °C in spitless mode. The oven temperature was maintained at 50 °C for ten minutes and was progressively increased to 310 °C at 2 °C/min. Coupled to the gas chromatograph was a DSQ Thermo mass

spectrometer with a heated interface (310 °C), electron energy of 70 eV and ion source at 220 °C, scanning from m/z 35 to 800 at 2 scans/s. Compounds were assigned on the basis of their mass spectra, comparison with the NIST library mass spectra, published mass spectra (e.g. Gallois *et al*. 2007; Templier *et al*. 2013) and GC retention times. The molecular structure of all compounds present in substantial amount was investigated without any ion selection that could have biased interpretations.

Institutional Abbreviation

YFGP: Yizhou Fossil and Geology Park; RBINS: Royal Belgian Institute of Natural Sciences; NIST: National Institute of Standards and Technology.

RESULTS

SEM/EDS and XRD

SEM of the fossil feathers revealed that they are embedded in a sedimentary matrix containing mainly quartz, carbonates, and phyllosilicates. The latter are organized in thin platelets oriented parallel to each other (Figs. 2A-B). A feather sample from the right wing of *Anchiornis* (sample 1 on Fig. 1) showed abundant rounded crystals that are present only beneath the surface. They occur mainly as framboids (Fig. 2C), but also as individual microcrystallites (Fig. 2D) and, in some cases, are associated with voids. Framboids are spheroidal or ovoid, 6 to 9 µm in diameter and contain dozens of euhedral crystals, 750 nm in diameter. In contrast, individual cubic crystals are much smaller (about 500 nm^3) and contain micro-crystallites (Fig. 2D). EDS analyses indicate that the sediment is composed of Fe, Si, O, Al, C, Ca

(and Mn, K, Mg), probably indicating the presence of quartz, calcite, and various phyllosilicates. XRD analyses confirmed the presence of these minerals in the sediment (Fig. 3A). In addition, the XRD spectrum of the < 2 μm phase shows that expansive material, such as illite and interstratified illite/smectite, is present in the sediment (Fig. 3B). Due to their characteristic framboidal shape and elemental composition, the crystal clusters observed beneath the fossil feather surface are attributed to diagenetic iron oxides or hydroxides. Indeed, although the framboidal habit is common for iron sulphides, the lack of sulphur here shows they are rather iron oxide pseudomorphs probably resulting from the *in situ* weathering of pyrite framboids (Blanco *et al*. 2013; Kaye *et al*. 2008; Nordstrom 1982; Wang *et al*. 2012). These structures are associated with thin clay overgrowths (arrow in Figs. 2C, E), indicating that the iron oxides (or the preceding pyrites) precipitated first. Tiny stellate minerals were also observed and identified as probable iron oxides by X-ray spectroscopy (Fig. 2F). The presence of calcium carbonates, feldspars (Fig. 2G) and quartz (Fig. 2H) in the sedimentary matrix was confirmed by X-ray spectroscopy.

Elongate microbodies, 650 to 950 μm, and their associated imprints were observed in three samples (6, 9, and 12, on Fig. 1) collected from the anterior and posterior parts of the dinosaur tail (Fig. 4). Microbody imprints are abundant, tightly packed together and randomly oriented (Figs. 4A–B). They likely represent traces of melanosomes. Similar microbodies interpreted as melanosomes have previously been observed in feathers from the crest of this specimen (YFGP-T5199; Lindgren *et al*. 2015). Here, isolated elongate structures were observed (Fig. 4C). These fossil organelles are preserved within the thin clay-rich sediment.

Ion Beam Analysis (IBA): EBS and PIXE

The great virtue of EBS is to be capable of yielding the elemental depth profiles non-destructively from the outermost microns of the sample with good sensitivity and depth resolution (Jeynes and Colaux 2016). A typical EBS spectrum obtained from the fossil feathers is shown in Supplementary Figure 3 together with its best fit. The experimental spectrum was inverted to recover the elemental depth profiles (examples are shown for carbon in Supplementary Fig. 4). Integration of these elemental depth profiles allows derivation of the concentration of each element at a given depth. Figure 5A clearly shows that the carbon enrichment in the near surface region (ca. 60%) decreases at increasing distance from the fossil feathers, reaching a minimum in the 'remote' sediment (ca. 14%). Sample concentrations of oxygen and silicon (although less obvious) follow an opposite trend. The nitrogen content in the modern buzzard feathers is ca. 20-26 %. The very low content of nitrogen in the fossil (ca. 5%) and even less (under the limit of detection) in the remote sediment (Supplementary Fig.3) precluded its depth profiling.

In contrast, EBS analysis of modern buzzard feathers shows homogeneous concentrations with depth (Supplementary Fig. 5). Carbon content in the buzzard feathers is about 60 at. %, while nitrogen and oxygen are both around 20 at. % for the rachis and around 25 and 15 at. % respectively for the barbs. Typical PIXE spectra acquired from the fossil feathers, 'host' sediment and 'remote' sediment are shown in Figure 5B. The samples differ in the amounts of several elements present (Supplementary Tables 1–2). Of particular interest is the sulphur content: there are elevated concentrations of sulphur in the fossil feathers (average 1,842 ± 208.5 ppm), less in the 'host' sediment (1,162 ± 143 ppm), and much lower concentrations in the 'remote' sediment (98 ± 35 ppm). The concentration of S in the fossil feathers is roughly twenty times lower (ca. 0.2 wt. %) than in the modern bird feathers (ca. 3.7 – 4.3 wt.

320 %). The co-occurrence between sulphur and carbon is also highlighted (Table 1). Both concentrations
321 decrease with depth within the fossil feathers whereas the reverse situation is observed for Si and O.

322

323 *^{13}C NMR*

324 The ^{13}C NMR spectrum of buzzard feathers (Fig. 6A) shows a complex signal in the aliphatic region,
325 with well-resolved peaks between 10 and 65 ppm and a narrow peak at 173 ppm, due to carboxyl
326 carbons, i.e. carboxylic groups and esters and amides. Two additional, less intense, signals can be seen
327 at 129 ppm and 158 ppm in the unsaturated/aromatic carbon region. In comparison to the spectrum of
328 modern feathers, the ^{13}C NMR spectra of the fossil feathers and their surrounding sediment show much
329 simpler patterns (Figs. 6B–C). The spectra are similar to each other and both are dominated by a broad
330 peak in the aliphatic region, maximizing at 30 ppm and thus indicative of long alkyl chains. Two
331 additional broad signals contribute to the spectra. The first one occurs as a broad shoulder between 68
332 and 80 ppm, in the O-alkyl C and N-alkyl C range, and the second one is a broad peak at 129 ppm,
333 attributed to aromatic carbons.

334

335 *Micro-ATR FTIR spectroscopy*

336 The micro-ATR FTIR spectra of the theropod feathers, the embedding sediment and the modern buzzard
337 feather (dark regions) are shown in figure 7.

338 The spectrum of the dark region of a modern buzzard feather shows characteristic bands of secondary
339 amides – as in proteins and polypeptides – at 1628 cm^{-1} (C=O stretch of Amide I), 1531 cm^{-1} (C-N
340 stretch, Amide II) and 1239 cm^{-1} (N-H in plane bending coupled with C-N stretch, Amide III). Broad

bands around 3274 and 3125 cm^{-1} can be attributed to the N-H stretching of secondary amides. The bands at 2961, 2922 and 2852 cm^{-1} are assigned to the C-H stretching of methylene and methyl groups. These two spectra are very similar and no significant differences could be found between IR response of the dark and white regions of the same feather.

The spectrum of the fossil feathers has a different pattern but some similarities with the modern buzzard feather appear. The distinct bands at 2920 and 2851 cm^{-1} can also be attributed to C-H stretching of methylene and methyl groups. These associated bands are also present in the IR spectrum of the surrounding matrix but with different relative intensities. A broad region around 3300 cm^{-1} is present, although much less marked, and is indicative for O-H stretching as found in carboxylic groups and alcohols. In the spectra of the fossil feathers, a broad band at about 1560 cm^{-1} can be attributed to carboxylate. This band is not present in IR spectrum of the sediment. Another broad band around 1412 cm^{-1} is found in the spectrum of the fossil feathers and might be related to the presence of $CaCO_3$ in overlap with C-H bending vibrations at 1460 and 1380 cm^{-1} (Andersen and Brečevic 1991; Kroner et al. 2010; Kiros et al. 2013) . This is also confirmed by the presence of weak bands at 873 and 718 cm^{-1}. The IR spectrum of the sediment shows a similar, but less defined, absorption band between 1415 and 1463 cm^{-1}. The IR spectrum of the fossil feathers and its surrounding matrix both show a narrow band at 1260 cm^{-1} that could be attributed to the Si-CH_3 vibrations. Both spectra show an intense broad band at 1013 cm^{-1} together with the weaker bands at 873 and 797 cm^{-1} related to the sedimentary matrix (clay minerals, quartz, silicates, Si-O stretching). The IR spectrum of the sedimentary matrix shows an additional band at 720 cm^{-1} that is also present, although very weak, in the fossil, indicating long-chain alkyl groups (CH_2 rocking vibrations). All the peaks mentioned above are absent in the IR spectra of the modern feather.

363

364 *TMAH Py-GC-MS*

365 Pyrochromatograms were obtained for the three following samples: the modern and fossil feathers, and
366 the 'host' sediment. In agreement with previous studies on bird feathers (Brebu and Spiridon 2011;
367 Saitta *et al*. 2017), the pyrochromatogram of the modern feathers is dominated by cyclic molecules
368 containing nitrogen, along with methylbenzene **1**, methylbutane nitriles **2, 3** and cyclohexanedione **11**
369 derivatives (Fig. 8A). Detailed interpretation of mass spectral fragmentation patterns allowed
370 identification of the major pyrolysis products (Table 2) and further assignment to possible source.
371 Molecular structures are given in Appendix, with methyl groups added by TMAH indicated in bold.
372 Products **6**, **8**, **10** result from direct methylation of alanine, valine and proline, thus pointing to a
373 proteinaceous origin for the feathers. This is further supported by the occurrence in substantial amounts
374 of alkylnitriles **2**, **3** resulting from dehydration of amides involving isoleucine and leucine, respectively,
375 and of methoxybenzenes **7**, **9** released through homolysis of the side chain of tyrosine (Ratcliff *et al*.,
376 1974). Methylbenzene **1**, pyrrole **4** and ethylbenzene **5** are rather ubiquitous pyrolysis products in
377 sedimentary organic matter. However, they can also be released upon pyrolysis of phenylalanine and
378 serine (Gallois *et al*. 2007). Mass spectral fragmentation pattern (base peak at m/z 82) suggests an origin
379 from the side chain of histidine for compound **16**. Similarly, compound **17** probably corresponds to a
380 valine derivative as its mass spectrum is characterized by the loss of 42 amu (i.e. valine side chain).
381 Dimethylcyclohexanedione **11** was reported as pyrolysis product of glycine (Moldoveanu 2009).
382 Glycine is also present as its diketopiperazine **15** resulting from combined dehydration and cyclisation
383 (Simmonds *et al*. 1972). The same mechanism involving two different amino acids (isoleucine-glycine)

leads to another diketopiperazine **18** (Hendricker and Voorhees 1996). The formation of more complex diketopiperazines was proposed by Templier *et al*. (2013) from tripeptide units. Similar mechanism can be invoked for the formation of compound **19** from valine, as well as compounds **20** and **21** from serine and leucine (Table 2; Supplementary Fig. 6). Imidazolidinedione **12** probably results from the internal cyclisation of tripeptide comprising an alanine unit as reported by Templier et al. (2013; Supplementary Fig. 6). The formation of imidazolidinone **13** can be related to the decomposition of bicyclic amidine derived from valine as suggested by Basiuk and Navarro-González (1997; Supplementary Fig. 6). Another decomposition pathway of bicyclic amidine is probably responsible for the formation of imidazolidinone **14** from valine and possibly glycine (Templier *et al*. 2013). As far as we know, this is the first identification of such complex molecules (diketopiperazines from tripeptide and imidazolidinone from bicyclic amidine) in the pyrolysate of a natural sample.

By comparison, pyrochromatograms of the fossil feathers and their 'host' sediment are simpler. They are dominated by *n*-alkane/*n*-alkene doublets (Figs. 8B–C), resulting from the homolytic cleavage of long alkyl chains. In the fossil feathers, these doublets comprise from 8 to 30 carbon atoms, and exhibit a smooth distribution except an intense C_{18} doublet. An additional series of fatty acid methyl esters with alkyl chain ranging from C_8 to C_{30} and maximizing at C_{16} is also identified (Table 2). It results from the release upon pyrolysis of a series of fatty acids that are methylated thanks to TMAH. In addition to these series, a methoxybenzene substituted by two methyl groups or an ethyl group **22** is detected in minor amounts, at the beginning of the pyrochromatogram. A trimethylbenzene and a methylated derivative of methoxyaniline **23** also contribute to this part of the pyrochromatogram. However, the most prominent pyrolysis product **24** corresponds to the C_{18} alcohol methylated through TMAH pyrolysis.

405 The pyrochromatogram of the "host" sediment shares several similarities with that of the fossil feathers.
406 Indeed, it is dominated by series of alkane/alkene doublets and fatty acid methyl esters. Although the
407 distribution of the fatty acid methyl esters is similar in both samples, that of the doublets differs. Indeed,
408 whereas their range ($C_8 - C_{30}$) is similar, the maximum of the series appears at C_{15} in the sediment,
409 instead of a marked predominance of the C_{18} in the fossil (Table 2). Moreover, when comparing the
410 minor compounds eluting at the beginning of the pyrochromatogram, compounds **22** and **23** are common
411 in both samples, whereas a higher number of alkylbenzene homologues occurs in the sediment. Finally,
412 the contribution of octadecanol **24** is much lower in the sediment pyrolysate.

413

414 **DISCUSSION**

415 *Ultrastructure*

416 Microbodies and elongate moulds are observed in feather samples collected at three different locations
417 on *Anchiornis* tail. The elongate shape, parallel orientation and location of the microbodies within the
418 feathers strongly suggest that they correspond to eumelanosomes. These pigment organelles are
419 associated to brown, grey and black hues in modern bird feathers. The preservation of melanosomes, and
420 especially eumelanosomes, in dinosaur feathers is not uncommon. Such microscopic melanin-bearing
421 structures have been described in other theropod dinosaurs, basal birds and isolated feathers (Li *et al*.
422 2010, 2012; Zhang *et al*. 2010; Carney *et al*. 2012; Colleary *et al*. 2015; Pan *et al*. 2016; Hu *et al*. 2018).
423 The chemical composition of these microbodies has been assessed in a previous study, confirming a
424 melanosome origin (Lindgren *et al.* 2015).

425 Recent taphonomic experiments in abiotic conditions suggest that the preservation of mouldic
426 melanosomes requires interaction with an oxidant prior to maturation, and that the preservation of
427 melanosomes is probably less frequent than the preservation of keratinous structures in fossil feathers
428 (Slater *et al*. 2020). It is interesting to see that *Anchiornis* feathers contain both melanosomes and
429 moulds, given their – anoxic – depositional setting. The abiotic nature of the former experiments does
430 however not reflect the depositional and fossilization conditions of *Anchiornis*.

431

432 *Depth profiling, light and heavy element composition*

433 The carbon and nitrogen concentrations determined by EBS led to N/C ratios of 0.33 to 0.42 in modern
434 buzzard feathers, and of 0.08 for the fossil, suggesting a marked relative decrease in nitrogen. The
435 carbon concentration gradient observed by EBS in the fossil feathers of *A. huxleyi* strongly suggests that
436 they are preserved as carbonaceous layers located at the uppermost part of the sample (i.e. 0 – 3 µm
437 depth, given a rock density of 2.65 g/cm³) and suggests that fossil organic matter could have
438 impregnated the sediment only in a nearby area.

439 The PIXE spectra show elevated concentrations of sulphur in the fossil feathers and, to a lesser extent, in
440 the 'host' sediment, together with very low concentrations in the 'remote' sediment. This suggests that S
441 is associated with the soft tissues. The fossil feathers are therefore preserved as a S-rich carbonaceous
442 film. Substantial quantities of sulphur are present in the modern buzzard feathers (43,070 ± 4,236 ppm
443 in the brown barbs and 37,142 ± 3,652 ppm in the rachis, Table 1). This is not surprising due to the
444 presence of sulphur-containing biomacromolecules, such as the pigment phaeomelanin and cysteine- or
445 methionine-containing proteins (i.e. keratins) in bird feathers (Bortolotti 2010; Cesarini 1996; Harrap

and Woods 1964; Murphy *et al*. 1990; Riley 1997; Saravanan and Dhurai 2012b). Important studies on the chemical composition of feathers have shown that S is a major element of bird feathers (Harrap and Wood, 1964, 1967; King and Murphy 1987; Murphy *et al*. 1990; Edwards *et al*. 2016). Some authors could even discriminate between organic S originating from keratin and phaeomelanin based on its speciation (Edwards *et al*. 2016). Previous *in situ* chemical analysis (TOF-SIMS) of the melanosomes from the present fossil revealed their enrichment in sulphur with respect to the surrounding sediment, but it could not determine whether it reflects the occurrence of phaeomelanin or diagenetic incorporation of sulphur in eumelanin (Lindgren *et al*. 2015). In a Cretaceous early bird, divalent elements (Cu, Ca, Zn) were suggested to form chelates with melanin (Wogelius *et al*. 2011). Such a complexation may have played a role in sulphur preservation in fossil soft tissues. Alternatively, the presence of sulphur in the fossil feathers can be attributed to natural sulphurization of the organic matter, i.e. the abiogenic intra-molecular incorporation of sulphur from the depositional environment during early diagenesis. The incorporation of sulphur into organic matter was interpreted as a way to enhance the preservation potential of certain labile substances through cross-linking (Sinninghe-Damsté and De Leeuw 1990; Sinninghe-Damsté *et al*. 1989; Sinninghe-Damsté *et al*. 1988; McNamara *et al*. 2016). Indeed, organic matter has the ability to form complexes with inorganic elements, including sulphur, which was traced in fossil soft tissues (e.g. Wogelius *et al*. 2011).

Functional groups in the organic matter

On the whole, the ^{13}C NMR and IR spectra of buzzard feathers (Fig. 6A and 7A) are comparable to that of several keratinous materials, such as feather keratin (Barone *et al*. 2005; Kricheldorf and Müller 1984; Wang and Cao 2012, Sharma et al. 2018), wool keratin (Yoshimizu and Ando 1990;

467 Wojciechowska *et al*. 2004) or gecko setae keratin (Jain *et al*. 2015). Indeed, the peak at 173 ppm should
468 mainly correspond to the signal of secondary amide (O=C-NH) groups involved in the peptidic bonds.
469 This is confirmed by the presence of characteristic bands of secondary amides in the IR spectrum of the
470 brown feathers (Fig. 7A). This includes a broad band around 3277 cm^{-1} attributed to the N-H stretching
471 band of amides, a narrow band at 1628 cm^{-1} related to the C=O stretch of Amide I, a band at 1518 cm^{-1}
472 attributed to Amide II and a band at 1237 cm^{-1} related to Amide III (e.g. Bendit 1966; Yu *et al*. 2004;
473 Wang and Cao 2012; Giraldo *et al*. 2013; Tesfaye *et al*. 2017).

474 Carbon atoms bearing both COOH and NH_2 groups (termed C_α) in the amino acids (except glycine)
475 resonate between 50 and 60 ppm in ^{13}C NMR. They account for the peaks at 52.9 and 60.2 ppm in the
476 broad aliphatic signal, whereas the signal at 42.6 ppm is assigned to the C_α of glycine. The other peaks
477 are mainly associated with the amino acid side chains, that at 30.8 ppm being assigned to C_β along with
478 C in long alkyl chains, and those at 19.8 and 25.7 ppm to C_γ and C_δ. The three bands located in the
479 2961-2850 cm^{-1} range in the IR spectra confirms the presence of aliphatic moieties in the modern
480 feathers, although their precise assignment to dedicated compounds is uncertain. In the ^{13}C NMR
481 spectrum, the 129 ppm peak is typical for aromatic carbons, including those from phenylalanine and
482 tyrosine (Jain *et al*. 2015; Yoshimizu and Ando 1990). Finally, the peak at 158 ppm can be ascribed to
483 the O-alkyl C of tyrosine and/or the C of the guanidino group (N-C=N) of arginine (Jain *et al*. 2015;
484 Yoshimizu and Ando 1990). This spectrum is in agreement with previous reports indicating that keratin
485 is a major constituent of feathers (Lucas and Stettenheim 1972). The ^{13}C NMR and IR spectra of the
486 modern feathers also shares some similarities with various types of melanins (Adhyaru *et al*. 2003; Duff
487 *et al*. 1988; Centeno and Shamir 2008; Ito and Nicol 1974).

488 The much simpler ^{13}C NMR spectra of the fossil feathers and their surrounding sediment are dominated
489 by long alkyl chains with a low contribution of aromatic carbons. This is also consistent with the IR
490 spectra (Fig. 7B), mainly showing contributions of aliphatics and silicate and carbonate minerals. When
491 compared to the ^{13}C spectrum of the modern feathers, the aliphatic signal in the fossil is poorly resolved;
492 the aromatic peak is broad and no resonance signal could be detected in the carboxylic region. These
493 features suggest that the proteinaceous contribution identified in the buzzard feathers is no longer
494 present in the fossil sample. The comparison between the FTIR spectrum of the modern feather and that
495 of the fossil feathers (Fig.7A)shows that the characteristic bands of amides are absent in the IR spectrum
496 of the fossil feathers. However, a more precise comparison can be achieved at the molecular level thanks
497 to pyrolysis in the presence of TMAH coupled with GC-MS.

498 *Molecular building blocks of organic matter*

499 TMAH Py-GC-MS analysis of modern feathers thus highlights the presence of glycine, serine, leucine,
500 alanine, valine and proline moieties in buzzard feather keratin, in agreement with previous studies on
501 feather keratin (Fig. 8A; Arai *et al*. 1983, 1986; Murphy *et al*. 1990; O'Donnell and Inglis 1974;
502 Saravanan and Dhurai 2012b; Staroń *et al*. 2011). Additionally, pyrolysis products derived from
503 isoleucine, phenylalanine and tyrosine occurred in substantial amounts although they are often
504 considered as minor constituents of feather keratin. However, homolysis of the side chain of
505 phenylalanine and tyrosine favours high yields in TMAH pyrolysis (Gallois *et al*. 2007). Despite its
506 acknowledged high abundance in feather keratin, cysteine is absent in the pyrochromatogram of buzzard
507 feathers, probably because it mainly releases H_2S upon pyrolysis (Moldoveanu 2009) not detected in the
508 presently used analytical conditions. Alternatively, some of the identified products (methylbenzene **1**,

methyl, methoxybenzene **9**) as well as glycine derivatives may originate from melanin, although they are poorly diagnostic compounds (Stępień *et al*. 2009). However, the melanin signal was reported to be overwhelmed by protein-derived products upon pyrolysis of bulk feathers (Barden *et al*. 2011).

The pyrochromatograms of the fossil feathers and their 'host' sediment are comparable as they are both dominated by series of alkane/alkene doublets and fatty acid methyl esters as well as minor compounds eluting at the beginning of the pyrochromatogram. The latter include a methoxybenzene substituted by two methyl groups or an ethyl group **22** which originates from lignin or polysaccharides such as cellulose, depending on its substitution pattern (Choi *et al*. 2013; Seitz and Ram 2000). Despite these similarities, differences are observed, including the much weaker abundance of octadecanol **24** in the sediment pyrolysate. These differences clearly show that even though some imprint from the sediment may have contributed to the fossil feather pyrolysate, at least some features are typical for the fossil feathers. They notably include the C_{18} doublet and octadecanol **24**. The predominance of the alkane/alkene doublets in the pyrolysate is in agreement with the strong aliphatic signal observed in NMR and FTIR (bands at 2690, 2920 and 2851 cm^{-1}) (Figs. 6–7). A similar highly aliphatic character has been reported in Eocene bird feathers (O'Reilly *et al*. 2017) but also in soft tissues from other fossil organisms, such as in cuticles from Carboniferous arthropods (Baas *et al*. 1995; Stankiewicz *et al*. 1998), skin from a Cretaceous mummified hadrosaur (Manning *et al*. 2009), and Cretaceous fish scales (Gupta *et al*. 2008). C_1 to C_3 alkylbenzenes were also identified in pyrolysates of Oligocene weevil and tadpole, and associated matrix (Barden *et al*. 2015; Gupta *et al*. 2007).

The aliphatic series dominating the pyrolysate of the fossil feathers reflect either selective preservation of macromolecular aliphatic matter pre-existing in the extant organism (Tegelaar *et al*. 1989) or *in situ*

polymerization of aliphatic lipids (Gupta *et al*. 2007; Stankiewicz *et al*. 2000). No such aliphatic series could be detected in the pyrolysate of modern feathers, likely precluding the first hypothesis. In contrast, several aliphatic series were identified in the lipid extract of the modern feathers (*n*-alkanes, *n*-acids, *n*-alcohols; data not shown). Indeed, modern bird feathers are coated by lipids as protection against adverse environmental factors. Such lipids, secreted by the uropygial gland, were recently shown to be preserved through geopolymerisation in an Eocene bird (O'Reilly *et al*. 2017). A similar geopolymerisation can be put forward to account for the occurrence of aliphatic moieties of the present fossil feathers. Endogenous lipids may be transformed into more stable geopolymers, composed of alkane/alkene doublets, and can therefore be 'preserved' and traced in vertebrate fossils (O'Reilly *et al*. 2018).

The absence of signals typical for proteinaceous material in the NMR and IR spectra and pyrochromatogram of the fossil feathers is noteworthy. It is further suggested by the weak N/C ratio in the fossil when compared with modern feathers. The lack of proteinaceous components consistent with keratin was previously suggested on the same fossil based on TOF-SIMS and IR analyses (Lindgren *et al*., 2015). In agreement with the commonly accepted lability of proteins, this feature suggests their extensive degradation in our specimen upon diagenesis. Recent taphonomy experiments on extant feathers demonstrated substantial degradation of keratin upon microbial and thermal decay (Saitta *et al*. 2017). Moreover, it must be noted that diagenetic degradation of proteinaceous moieties was previously put forward for Eocene birds (Saitta *et al*. 2017; O'Reilly *et al*. 2017) and Palaeozoic annelid fossils (Dutta *et al*. 2010). However, even if no proteinaceous compounds were detected in *Anchiornis* feathers, one cannot exclude the possibility of finding similar biomolecules preserved in other fossils in the future.

552 Although PIXE analyses showed that carbon and sulphur are closely associated in the fossil feathers, no
553 organosulphur compound could be detected in the pyrolysate. Altogether, the lack of organosulphur
554 compounds (such as thiophenes) in the fossil feather pyrolysates and the lack of C=S/C-S species in
555 their IR spectrum strongly suggest a lack of organic-S species in this sample. In contrast, sulphur
556 incorporation was evidenced through FTIR and TMAH-Py-GC-MS in melanosomes of Miocene frogs,
557 thus demonstrating involvement of natural sulphurization in the preservation of the fossil organic matter
558 (McNamara *et al*., 2016). The lack of organosulphur compounds in *Anchiornis* pyrolysate should thus
559 reflect diagenetic conditions that prevented such natural sulphurization of organic matter. In the
560 sedimentary environment, the sulphurization of organic matter to form organosulphur compounds
561 requires the presence of reactive organic matter and inorganic sulphides (i.e. anoxic conditions), with
562 sufficient, but not excessive, reactive iron. If reactive iron exceeds a certain quantity, iron sulphides
563 (pyrite) would precipitate instead (Werne *et al*. 2000; Canfield 1989). Here, our results suggest that the
564 concentration of sulphur and iron in the environment was high enough to form iron sulphides (i.e. pyrite
565 framboids and microcrystallites). The occurrence of iron oxides or hydroxides as framboid crystals
566 (SEM and EDX characterization) suggests that sulphur may have been preferentially used for the
567 formation of iron sulphides (such as pyrite) during early diagenesis (Sinninghe-Damsté and De Leeuw
568 1990). During later diagenesis, pyrite framboids were probably *in situ* weathered into the iron oxides and
569 hydroxides observed beneath the carbonaceous surface of feathers, thus releasing sulphur that may have
570 been further associated with organic compounds, e.g. through the formation of chelate with melanin
571 (Wogelius *et al*. 2011). Such associations may have favoured/enhanced organic matter preservation and
572 are consistent with the interrelation between sulphur and carbon highlighted by PIXE analyses.

573 Recently, a mechanism of nitrogen preservation based on lipoxidation and glycoxidation of protein was
574 proposed in biomineralized tissues of diverse Mesozoic and Cenozoic vertebrates, fossilized in oxidative
575 settings (Wiemann *et al*. 2018). Such a process, which can be catalysed by transition metal such as iron,
576 may have led to the preservation of the small amount of nitrogen in YFGP-T5199. However, the present
577 study deals with soft tissues and not biomineralized one. Additionally, so far this preservation
578 mechanism could only be evidenced in oxidizing environment (Wiemann *et al*. 2018). The occurrence of
579 iron oxide framboids in the studied *Anchiornis* fossil probably resulting from pyrite weathering, rather
580 attests for the reducing conditions of fossilisation, thus making unlikely the involvement of this
581 preservation pathway (i.e. lipoxidation).

582 Further experimental studies on modern feathers and comparisons with the fossil record are required to
583 explain why keratin is not preserved in *Anchiornis* feathers although melanin has been detected, and
584 melanosomes and moulds have been observed.

585

586 **CONCLUSIONS**
587

588 The methods used in this study provide new and complementary information on how the plumage of
589 *Anchiornis huxleyi* (YFGP-T5199) is preserved. SEM and EDS reveal that fossil feathers are preserved
590 in a fine-grained material constituted of K-rich phyllosilicates, illite and interstratified illite/smectite.
591 PIXE analyses show that both light (C, N, O) and heavy (S, Na, Ca, etc.) elements are present in the
592 fossil samples, even at very low concentrations. The presence of iron oxide pseudomorphs after pyrite
593 likely indicates a reduced depositional environment for *Anchiornis*. Carbon is the dominant element in

the fossil feathers, which are also enriched in sulphur with respect to the 'host' sediment. EBS mapping of the interior of the samples revealed a decrease in carbon concentration with depth. Our analysis therefore shows that the fossil feathers are preserved in the uppermost part of the sample, as a thin – ca. 3 µm-thick – S-bearing carbonaceous layer. High resolution imaging of the feather microstructure revealed the presence of elongated microbodies (650-950 nm), likely corresponding to eumelanosomes. Molecular characterization of the organic matter in the 'host' sediment, fossil feathers and modern feathers by ^{13}C-NMR, micro-ATR FTIR and Py-GC-MS shows that the fossil does not display the complex amino-acid signature typical for keratin, the main constituent of modern feathers. Although the organic matter of the fossil feathers and their 'host' sediment are both dominated by aliphatic moieties, they exhibit substantial differences (distribution pattern of series, occurrence of components specific to the feathers) suggesting that the organic matter of the fossil feathers is derived, at least partially, from original constituents of the feathers.

Altogether, these results show that the fossil feathers can be described as compression fossils, as described in Schweitzer (2011: p. 192). The finely grained (clay-rich) host sediment contributed to the morphological preservation of *Anchiornis* soft tissues. As stressed by Schweitzer (2011: p. 192), the very fine grain size of the sediments might have prevented the degradation of soft tissues by microbes, and subsequent loss of degraded organic matter in the environment before and during diagenesis. However, the lack of protein-derived moieties in the fossil organic matter shows that the latter has been significantly altered during diagenesis. The excellent morphological preservation of the fossil soft tissue is not associated here with a high preservation level of organic matter. Hence, the fossil feathers have likely undergone a complex diagenetic history including several steps affecting differentially their morphology and chemistry. *In situ* polymerization of lipids into more stable aliphatic compounds during

early diagenesis was likely the main process responsible for organic matter preservation in the fossil feathers. Additionally, sulphur was probably involved in several steps of the fossil preservation although no natural sulphurization took place.

Our results are therefore unique by combining different analytical techniques on Jurassic fossil feathers. This integrative multidisciplinary study appears as a powerful approach to decipher morphological, mineralogical, structural and chemical features of fossil soft tissues and their fossilization processes.

This study provides new insights into the taphonomy of labile compounds, suggesting that keratin, unlike the pigment melanin, is not present in the feathers of YFGP- T5199.Our results question the preservation potential of keratin (and melanin) in anoxic conditions. Further analyses of fossil feathers of different ages and deposited in different environmental settings, are required to better understand the preservation potential of melanin and keratin.

Finally, we used here for the first time on a Jurassic fossil Ion Beam Analysis (IBA), a non-destructive analytical technique providing an in-depth profiling of C to U elements. Further developments of this technique to palaeontological samples might help at identifying the precise location of fossil soft tissues within the sediment and then characterizing metal elements that are directly associated with the fossilised tissues.

Acknowledgements. This work was made possible through a FRIA grant provided to A. C. by the 'Fonds National pour la Recherche Scientifique' (F.R.S. - F.N.R.S.). Gaëtan Rochez (UNamur) is thanked for his technical support in XRD analyses. Julien Cillis and Thierry Leduc (RBINS) are thanked for their

grateful help in SEM image acquisition and EDS analyses. Maria McNamara (UCC) is warmly thanked for her advice and comments. We also thank Dr Geoffrey Grime of the Ion Beam Centre, University of Surrey, UK, for his valuable advices regarding the PIXE measurements. A.C. is currently funded by the Irish Research Council (GOIPD/2018/768). The authors wish to thank both anonymous reviewers whose comments greatly helped to improve this manuscript.

DATA ARCHIVING STATEMENT

Additional data for this study are available in the [Dryad Digital Repository]: https://datadryad.org/review?doi=doi:10.5061/dryad.XXXX

REFERENCES

ADHYARU, B. B., AKHMEDOV, N. D., KATRITZKY, A. R. and BOWERS, C. R. 2003. Solid-state cross-polarization magic angle spinning ^{13}C and ^{15}N NMR characterization of Sepia melanin, Sepia melanin free acid and Human hair melanin in comparison with several model compounds. *Magnetic resonance in chemistry*, **41**, 466-474.

ALLISON, P. A. and BRIGGS, D. E. G. 1993. Exceptional fossil record: Distribution of soft-tissue preservation through the Phanerozoic. *Geology*, **21**, 527-532.

ARAI, K. M., TAKAHASHI, R., YOKOTE, Y. and AKAHANE, K. 1983. Amino acid sequence of feather keratin from fowl. *The FEBS Journal*, **132** (3), 501-507.

—— 1986. The primary structure of feather keratins from duck (*Anas platyrhynchos*) and pigeon (*Columba livia*). *Biochimica et Biophysica Acta (BBA)-Protein Structure and Molecular Enzymology*, **873** (1), 6-12.

BAAS, M., BRIGGS, D., VAN HEEMST, J., KEAR, A. and DE LEEUW, J. 1995. Selective preservation of chitin during the decay of shrimp. *Geochimica et Cosmochimica Acta*, **59** (5), 945-951.

BARDEN, H. E., WOGELIUS, R. A., LI, D., MANNING, P. L., EDWARDS, N. P. and VAN DONGEN, B. E. 2011. Morphological and geochemical evidence of eumelanin preservation in the feathers of the Early Cretaceous bird, *Gansus yumenensis*. *PLoS One*, **6** (10), e25494

BARDEN, H. E., BERGMANN, U., EDWARDS, N. P., EGERTON, V. M., MANNING, P. L., PERRY, S., VAN VEELEN, A., WOGELIUS, R. A. and VAN DONGEN, B.E. 2015. Bacteria or melanosomes? A geochemical analysis of micro-bodies on a tadpole from the Oligocene Enspel Formation of Germany. *Palaeobiodiversity and Palaeoenvironments*, **95** (1), 33-45.

BARONE, J. R., SCHMIDT, W. F. and LIEBNER, C. F. E. 2005. Thermally processed keratin films. *Journal of Applied Polymer Science*, **97**, 1644-1651.

BARTHEL, K. 1964. Zur Entstehung der Solnhofer Plattenkalke (unteres Untertithon). *Mitteilungen der Bayerischen Staatssammlung für Paläontologie und Historische Geologie*, **4**, 37-69.

BASIUK, V. A. and NAVARRO-GONZÁLEZ, R. 1997. Identification of hexahydroimidazo [1, 2-a] pyrazine-3, 6-diones and hexahydroimidazo [1, 2-a] imidazo [1, 2-d] pyrazine-3, 8-diones, unusual products of silica-catalyzed amino acid thermal condensation and products of their thermal decomposition using coupled high-performance liquid chromatography–particle beam

mass spectrometry and gas chromatography–Fourier transform infrared spectroscopy–mass spectrometry. *Journal of Chromatography A*, **776** (2), 255-273.

BECK, L. 2014. Recent trends in IBA for cultural heritage studies. *Nuclear Instruments and Methods in Physics Research B*, **332**, 439-444.

BENDIT, E.G. 1966. Infrared absorption spectrum of keratin. I. Spectra of α-, β-, and supercontracted keratin. *Biopolymers*, **4**, 539-559.

BENTON, M. J., ZHONGHE, Z., ORR, P. J., FUCHENG, Z. and KEARNS, S. L. 2008. The remarkable fossils from the Early Cretaceous Jehol Biota of China and how they have changed our knowledge of Mesozoic life. *Proceedings of the Geologists' Association*, **119**, 209-229.

BLANCO, A., BOLAÑOS-SÁNCHEZ, U., LIZÁRRAGA-MENDIOLA, L., HERNÁNDEZ-ÁVILA, J., ÁNGELES-TRIGUEROS, S., AMBROCIO, P. and GONZÁLEZ-SANDOVAL, M. 2013. Microscopic evidences of replacement of iron sulfide by iron oxide in macro fossils: a useful tool for the search of life in Mars? *Lunar and Planetary Science Conference*, **44**, 2956.

BORTOLOTTI, G. R. 2010. Flaws and pitfalls in the chemical analysis of feathers: bad news–good news for avian chemoecology and toxicology. *Ecological Applications*, **20** (6), 1766-1774.

BRIGGS, D. E. G., KEAR, A., MARTILL, D. and WILBY, P. 1993. Phosphatization of soft-tissue in experiments and fossils. *Journal of the Geological Society*, **150** (6), 1035-1038.

BRIGGS, D. E. G., BOTTRELL, S. H. and RAISWELL, R. 1991. Pyritization of soft-bodied fossils: Beecher's trilobite bed, Upper Ordovician, New York State. *Geology*, **19** (12), 1221-1224.

BUTTERFIELD, N. J., BALTHASAR, U. and WILSON, L. A. 2007. Fossil diagenesis in the Burgess Shale. *Palaeontology*, **50** (3), 537-543.

699 CAMPBELL, J., BOYD, N., GRASSI, N., BONNICK, P. and MAXWELL, J. 2010. The Guelph PIXE
700 software package IV. *Nuclear Instruments and Methods in Physics Research Section B: Beam*
701 *Interactions with Materials and Atoms*, **268** (20), 3356-3363.
702 CANFIELD, D. E. 1989. Reactive iron in marine sediments. *Geochemica and Cosmochemica Acta*, **53**
703 **(3**), 619-632.
704 CENTENO, S. A. and SHAMIR, J. 2008. Surface enhanced Raman scattering (SERS) and FTIR
705 characterization of the sepia melanin pigment used in works of art. *Journal of Molecular*
706 *Structure*, **873** (1-3), 149-159.
707 CESARINI, J. P. 1996. Melanins and their possible roles through biological evolution. *Advances in*
708 *space research*, **18** (12), 35-40.
709 CHANG, S. C., ZHANG, H., RENNE, P. R. and FANG, Y. 2009. High-precision $^{40}Ar/^{39}Ar$ age
710 constraints on the basal Lanqi Formation and its implications for the origin of angiosperm plants.
711 *Earth and Planetary Science Letters*, **279** (3), 212-221.
712 CHOI, S. S., KIM, M. C. and KIM, Y. K. 2013. Formation of methoxybenzenes from cellulose in the
713 presence of tetramethylammonium hydroxide by pyrolysis. *Bulletin of the Korean Chemical*
714 *Society*, **34** (2), 649-652.
715 CHRISTIANSEN, P. and BONDE, N. 2004. Body plumage in *Archaeopteryx*: a review and new
716 evidence from the Berlin specimen. *Comptes Rendus Palevol*, **3** (2), 99-118.
717 CHU, Z., HE, H., RAMEZANI, J., BOWRING, S. A., HU, D., ZHANG, L., ZHENG, S., WANG, X.,
718 ZHOU, Z. and DENG, C. 2016. High-precision U-Pb geochronology of the Jurassic Yanliao
719 Biota from Jianchang (western Liaoning Province, China): Age constraints on the rise of

feathered dinosaurs and eutherian mammals. *Geochemistry, Geophysics, Geosystems*, **17** (10), 3983-3992.

CINCOTTA, A., PESTCHEVITSKAYA, E. B., SINITSA, S. M., MARKEVICH, V. S., DEBAILLE, V., RESHETOVA, S. A., MASHCHUK, I. M., FROLOV, A. O., GERDES, A., YANS, J. and GODEFROIT, P. 2019. The rise of feathered dinosaurs: Kulindadromeus zabaikalicus, the oldest dinosaur with 'feather-like'structures. *PeerJ*, **7**, e6239.

COLLEARY, C., DOLOCAN, A., GARDNER, J., SINGH, S., WUTTKE, M., RABENSTEIN, R., HABERSETZER, J., SCHAAL, S., FESEHA, M. and CLEMENS, M. 2015. Chemical, experimental, and morphological evidence for diagenetically altered melanin in exceptionally preserved fossils. *Proceedings of the National Academy of Sciences*, **112** (41), 12592-12597.

DAVIS, J. A. 1984. Complexation of trace metals by adsorbed natural organic matter. *Geochimica et Cosmochimica Acta*, **48** (4), 679-691.

DUFF, G. A., ROBERTS, J. E. and FOSTER, N. 1988. Analysis of the structure of synthetic and natural melanins by solid-phase NMR. *Biochemistry*, **27**, 7112-7116.

DUTTA, S., HARTKOPF-FRÖDER, C., MANN, U., WILKES, H., BROCKE, R. and BERTRAM, N. 2010. Macromolecular composition of Palaeozoic scolecodonts: insights into the molecular taphonomy of zoomorphs. *Lethaia*, **43** (3), 334-343.

FARRELL, Ú. C., BRIGGS, D. E. G., HAMMARLUND, E. U., SPERLING, E. A. and GAINES, R. R. 2013. Paleoredox and pyritization of soft-bodied fossils in the Ordovician Frankfort Shale of New York. *American Journal of Science*, **313** (5), 452-489.

FRASER, R. D. B. and MACRAE, T. P. 2012. *Conformation in fibrous proteins and related synthetic polypeptides*. Academic press, London, 648 pp.

742 FRASER, R. D. B. and PARRY, D. A. D. 1996. The molecular structure of reptilian keratin.
743 *International Journal of Biological Macromolecules*, **19** (3), 207-211.
744 GABBOTT, S., NORRY, M., ALDRIDGE, R. and THERON, J. 2001. Preservation of fossils in clay
745 minerals; a unique example from the Upper Ordovician Soom Shale, South Africa. *Proceedings*
746 *of the Yorkshire Geological Society*, **53** (3), 237-244.
747 GALLOIS, N., TEMPLIER, J. and DERENNE, S. 2007. Pyrolysis-gas chromatography-mass
748 spectrometry of the 20 protein amino acids in the presence of TMAH. *Journal of Analytical and*
749 *Applied Pyrolysis*, **80**, 216-230.
750 GODEFROIT, P., CAU, A., DONG-YU, H., ESCUILLIÉ, F., WENHAO, W. and DYKE, G. 2013. A
751 Jurassic avialan dinosaur from China resolves the early phylogenetic history of birds. *Nature*,
752 **498 (7**454), 359-362.
753 GODEFROIT, P., SINITSA, S. M., DHOUAILLY, D., BOLOTSKY, Y. L., SIZOV, A. V.,
754 MCNAMARA, M. E., BENTON, M. J. and SPAGNA, P. 2014. A Jurassic ornithischian
755 dinosaur from Siberia with both feathers and scales. *Science*, **345** (6).
756 GODEFROIT, P., SINITSA, S. M., CINCOTTA, A., MCNAMARA M. E., RESHETOVA, S. A. and
757 DHOUAILLY, D. 2020. Integumentary structures in *Kulindadromeus zabaikalicus*, a Basal
758 Neornithischian Dinosaur from the Jurassic of Siberia. In FOTH, C. and RAUHUT, O. W. M.
759 (eds.). *The Evolution of Feathers*. Springer, Switzerland, 47-65.
760 GRADSTEIN, F. M., OGG, J. G., SCHMITZ, M. and OGG, G. 2012. The geologic time scale 2012.
761 Elsevier.

GREGG, K. and ROGERS, G. E.. 1986. Feather keratin: composition, structure and biogenesis. *In* BEREITER-HAHN, J., MATOLSKY, A. G. and RICHARDS, K. S. (eds). *Biology of the integument*. Springer, Berlin, Heidelberg, 666-694.

GUPTA, N. S., CAMBRA-MOO, O., BRIGGS, D. E., LOVE, G. D., FREGENAL-MARTINEZ, M. A. and SUMMONS, R. E. 2008. Molecular taphonomy of macrofossils from the Cretaceous Las Hoyas Formation, Spain. *Cretaceous Research*, **29** (1), 1-8.

GUPTA, N. S., MICHELS, R., BRIGGS, D. E., COLLINSON, M. E., EVERSHED, R. P. and PANCOST, R. D. 2007. Experimental evidence for the formation of geomacromolecules from plant leaf lipids. Organic *Geochemistry*, **38** (1), 28-36.

GURBICH, A. 2016. SigmaCalc recent development and present status of the evaluated cross-sections for IBA. *Nuclear Instruments and Methods in Physics Research Section B: Beam Interactions with Materials and Atoms*, **371**, 27-32.

HARMS, F. 2002. Steine erzählen Geschichte (n): Ursache für die Entstehung des Messel-Sees gefunden. *Natur und Museum*, **132** (1), 1-4.

HARRAP, B. S. and WOODS, E. F. 1964. Soluble derivatives of feather keratin: 1. Isolation, fractionation and amino acid composition. *Biochemical journal*, **92** (1), 8.

— 1967. Species differences in the proteins of feathers. *Comparative Biochemistry and Physiology*, **20** (2), 449-460

HENDRICKER, A. D. and VOORHEES, K. J. 1996. An investigation into the Curie-point pyrolysis-mass spectrometry of glycyl dipeptides. *Journal of Analytical and Applied Pyrolysis*, **36** (1), 51-70.

783 HEIMHOFER, R. and MARTILL, D. 2007. The sedimentology and depositional environment of the
784 Crato Formation. *In* MARTILL, D. M., BECHLY, G. and LOVERIDGE, R. F. (eds). *The Crato*
785 *fossil beds of Brazil: a window into an ancient world*. Cambridge University Press, 44-62.
786 HU, D., HOUL, L., ZHANG, L. and XU, X. 2009. A pre-*Archaeopteryx* troodontid theropod from
787 China with long feathers on the metatarsus. *Nature*, **461** (7264), 640.
788 ITO, S. and NICOL, J. C. 1974. Isolation of oligomers of 5, 6-dihydroxyindole-2-carboxylic acid from
789 the eye of the catfish. *Biochemical Journal*, **143** (1), 207-217.
790 JAIN, D., STARK, A. Y., NIEWIAROWSKI, P. H., MIYOSHI, T. and DHINOJWALA, A. 2015. NMR
791 spectroscopy reveals the presence and association of lipids and keratin in adhesive gecko setae.
792 *Scientific Reports,* **5** (9594).
793 JEYNES, C., BARRADAS, N., MARRIOTT, P., BOUDREAULT, G., JENKIN, M., WENDLER, E.
794 and WEBB, R. 2003. Elemental thin film depth profiles by ion beam analysis using simulated
795 annealing-a new tool. *Journal of Physics D: Applied Physics*, **36** (**7**0), R97.
796 JEYNES, C. and COLAUX, J. L. 2016. Thin film depth profiling by ion beam analysis. *Analyst*, **141**
797 (21), 5944-5985.
798 JI, Q. and JI, S. 1996. On the Discovery of the earliest fossil bird in China (*Sinosauropteryx* gen. nov.)
799 and the origin of birds. *Chinese Geology*, **233**, 6.
800 KAYE, T. G., GAUGLER, G. and SAWLOWICZ, Z. 2008. Dinosaurian soft tissues interpreted as
801 bacterial biofilms. *PLoS ONE*, **3** (7), e2808.
802 KELLNER, A. W., WANG, X., TISCHLINGER, H., DE ALMEIDA CAMPOS, D., HONE, D. W. and
803 MENG, X. 2010. The soft tissue of Jeholopterus (Pterosauria, Anurognathidae,

804 Batrachognathinae) and the structure of the pterosaur wing membrane. *Proceedings of the Royal*
805 *Society of London B: Biological Sciences*, **277** (1679), 321-329.
806 KELLNER, A. W. A. and DE ALMEIDA CAMPOS, D. 2002. The function of the cranial crest and jaws
807 of a unique pterosaur from the Early Cretaceous of Brazil. *Science*, **297**, 389-392.
808 KING, J. R. and MURPHY, M. E. 1987. Amino acid composition of the calamus, rachis, and barbs of
809 white-crowned sparrow feathers. *The Condor*, **89** (2), 436-439.
810 KRICHELDORF, H. R. and MÜLLER, D. 1984. Secondary structure of peptides 16th. Characterization
811 of proteins by means of ^{13}C NMR CP/MAS spectroscopy. *Colloid & Polymer Science*, **262**, 856-
812 861.
813 LENG, Q. and YANG, H. 2003. Pyrite framboids associated with the Mesozoic Jehol biota in
814 northeastern China: implications for microenvironment during early fossilization. *Progress in*
815 *Natural Science*, **13** (3), 206-212.
816 LI, Q., GAO, K. -Q., VINTHER, J., SHAWKEY, M. D., CLARKE, J. A., D'ALBA, L., MENG, Q.,
817 BRIGGS, D. E. G. and PRUM, R. O. 2010. Plumage color patterns of an extinct dinosaur.
818 *Science*, **327**, 1369-1372.
819 LI, Q., GAO, K. -Q., MENG, Q., CLARKE, J. A., SHAWKEY, M. D., D'ALBA, L., PEI, R.,
820 ELLISON, M., NORELL, M. A. and VINTHER, J. 2012. Reconstruction of *Microraptor* and the
821 evolution of iridescent plumage. *Science*, **335**, 1215.
822 LINDGREN, J., SJÖVALL, P., CARNEY, R. M., CINCOTTA, A., UVDAL, P., HUTCHESON, S. W.,
823 GUSTAFSSON, O., LEFÈVRE, U., ESCUILLIER, F., HEIMDAL, J., ENGDAHL, A., GREN,
824 J. A., KEAR, B. P., WAKAMATSU, K., YANS, J. and GODEFROIT, P. 2015. Molecular
825 composition and ultrastructure of Jurassic paravian feathers. *Scientific Reports*, 5(13520).

826 LIU, Y. Q., KUANG, H. W., JIANG, X. J., PENG, N., XU, H. and SUN, H. Y. 2012. Timing of the
827 earliest known feathered dinosaurs and transitional pterosaurs older than the Jehol Biota.
828 *Palaeogeography, Palaeoclimatology, Palaeoecology*, **323-325**, 1-12.
829 LUCAS, A. M., and P. R. STETTENHEIM. 1972. *Avian anatomy: Integuments*. U.S. Department of
830 Agriculture in cooperation with Michigan Agricultural Experiment Station, Washington D.C.
831 MANNING, P. L., P. M. MORRIS, A. MCMAHON, E. JONES, A. GIZE, J. H. MACQUAKER, G.
832 WOLFF, A. THOMPSON, J. MARSHALL, and K. G. TAYLOR. 2009. Mineralized soft-tissue
833 structure and chemistry in a mummified hadrosaur from the Hell Creek Formation, North Dakota
834 (USA). *Proceedings of the Royal Society of London B: Biological Sciences*, **276** (1672), 3429-
835 3437.
836 MANNING, P. L., N. P. EDWARDS, R. A. WOGELIUS, U. BERGMANN, H. E. BARDEN, P. L.
837 LARSON, D. SCHWARZ-WINGS, V. M. EGERTON, D. SOKARAS, and R. A. MORI. 2013.
838 Synchrotron-based chemical imaging reveals plumage patterns in a 150 million year old early
839 bird. *Journal of Analytical Atomic Spectrometry*, **28** (7), 1024-1030.
840 MARTILL, D. M. and HEIMHOFER, U. 2007. Stratigraphy of the Crato Formation. *In* MARTILL, D.
841 M., BECHLY, G. and LOVERIDGE, R. F. *The Crato fossil beds of Brazil: window into an*
842 *ancient world*. Cambridge University Press, 25-43.
843 MARTIN, D., BRIGGS, D. E. and PARKES, R. J. 2004. Experimental attachment of sediment particles
844 to invertebrate eggs and the preservation of soft-bodied fossils. *Journal of the Geological*
845 *Society*, **161** (5), 735-738.
846 MAYR, G., PETERS, D. S., PLODOWSKI, G. and VOGEL, O. 2002. Bristle-like integumentary
847 structures at the tail of the horned dinosaur *Psittacosaurus*. *Naturwissenschaften*, **89**, 361-365.

MCNAMARA, M. E., VAN DONGEN, B. E., LOCKYER, N. P., BULL, I. D. and ORR, P. J. 2016. Fossilization of melanosomes via sulfurization. *Palaeontology,* **59** (3), 1-14.

MOLDOVEANU, S. C. 2009. Pyrolysis of organic molecules: applications to health and environmental issues. *In* techniques and instrumentation in analytical chemistry, Elsevier, **28**, 723pp.

MOYER, A. E., ZHENG, W. and SCHWEITZER, M. H. 2016. Keratin durability has implications for the fossil record: results from a 10 year feather degradation experiment. *PloS One,* **11** (7), e0157699.

MURPHY, M. E., KING, J. R., TARUSCIO, T. G. and GEUPEL, G. R. 1990. Amino acid composition of feather barbs and rachises in three species of pygoscelid penguins: nutritional implications. *The Condor,* **92** (4), 913-921.

NAN, P., YONGQING, L., HONGWEI, K., XIAOJUN, J. and HUAN, X. 2012. Stratigraphy and geochronology of vertebrate fossil-bearing Jurassic strata from Linglongta, Jianchang County, Western Liaoning, Northeastern China. *Acta Geologica Sinica* (English Edition), **86** (6), 1326-1339.

NORDSTROM, D. K. 1982. Aqueous pyrite oxidation and the consequent formation of secondary iron minerals. *In* KITTRICK, J. A., FANNING, D. S. and HOSSNER, L. R. (eds), *Acid Sulfate Weathering*. Soil Science Society of America, Spec. Publ. 10, Madison, 37-56.

O'DONNELL, I. and INGLIS, A. 1974. Amino acid sequence of a feather keratin from Silver Gull (*Larus novae-hollandiae*) and comparison with one from Emu (*Dromaius novae-hollandiae*). *Australian journal of biological sciences,* **27** (4), 369-382.

O'REILLY, S., SUMMONS, R., MAYR, G. and VINTHER, J. 2018. Preservation of uropygial gland lipids in a 48-million-year-old bird. *Proceedings of the Royal Society B,* **284**, 20071050.

PAN, Y., SHA, J., ZHOU, Z. and FÜRSICH, F. T. 2013. The Jehol Biota: definition and distribution of exceptionally preserved relicts of a continental Early Cretaceous ecosystem. *Cretaceous Research*, **44**, 30-38.

PAN, Y., ZHENG, W., MOYER, A. E., O'CONNOR, J. K., WANG, M., ZHENG, X., Wang, X., SCHROETER, E. R., ZHOU, Z. and SCHWEITZER, M. H. 2016. Molecular evidence of keratin and melanosomes in feathers of the Early Cretaceous bird Eoconfuciusornis. *Proceedings of the National Academy of Sciences*, **113** (49), E7900-E7907.

PAN, Y., ZHENG, W., SAWYER, R. H., PENNINGTON, M. W., ZHENG, X., WANG, X., WANG, M., HU, L., O'CONNOR, J., ZHAO, T. and LI, Z. 2019. The molecular evolution of feathers with direct evidence from fossils. *Proceedings of the National Academy of Sciences*, **116** (8), 3018-3023.

RAUHUT, O. W., FOTH, C., TISCHLINGER, H. and NORELL, M. A. 2012. Exceptionally preserved juvenile megalosauroid theropod dinosaur with filamentous integument from the Late Jurassic of Germany. *Proceedings of the National Academy of Sciences*, **109** (29), 11746-11751.

RILEY, P. A. 1997. Melanin. *The international journal of biochemistry & cell biology*, **29** (11), 1235-1239.

SAITTA, E.T., ROGERS, C., BROOKER, R.A., ABBOTT, G.D., KUMAR, S., O'REILLY, S.S., DONOHOE, P., DUTTA, S., SUMMONS, R.E. and VINTHER, J. 2017. Low fossilization potential of keratin protein revealed by experimental taphonomy. *Palaeontology*, **60** (4), 547-556.

SARAVANAN, K. and DHURAI, B. 2012. Exploration on amino acid content and morphological structure in chicken feather fiber. *Journal of Textile and Apparel, Technology and Management*, **7** (3), 1-6.

SCHWEITZER, M. H., WATT, J. A., AVCI, R., FORSTER, C. A., KRAUSE, D. W., KNAPP, L., ROGERS, R. R., BEECH, I. and MARSHALL, M. 1999. Keratin immunoreactivity in the Late Cretaceous bird *Rahonavis ostromi*. *Journal of Vertebrate Paleontology*, **19** (4), 712-722.

SCHWEITZER, M. H. 2011. Soft tissue preservation in terrestrial Mesozoic vertebrates. Annual Review of *Earth and Planetary Sciences*, **39**, 187-216.

SEITZ, L. M. and RAM, M. 2000. Volatile methoxybenzene compounds in grains with off-odors. *Journal of agricultural and food chemistry*, **48** (9), 4279-4289.

SHARMA, S., GUPTA, A., KUMAR, A., KEE, C. G., KAMYAB, H. and SAUFI, S. M. 2018. An efficient conversion of waste feather keratin into ecofriendly bioplastic film. *Clean Technologies and Environmental Policy*, **20** (10), 2157-2167.

SIMMONDS, P., MEDLEY, E., RATCLIFF, M. and SHULMAN, G. 1972. Thermal decomposition of aliphatic monoaminomonocarboxylic acids. *Analytical chemistry*, **44** (12), 2060-2066.

SINNINGHE-DAMSTÉ, J. S. and DE LEEUW, J. W. 1990. Analysis, structure and geochemical significance of organically-bound sulphur in the geosphere: state of the art and future research. *Organic Geochemistry*, **16** (4-6), 1077-1101.

SINNINGHE-DAMSTÉ, J. S., EGLINTON, T. I., RIJPSTRA, W. I. C. and DE LEEUW, J. W. 1990. Molecular characterization of organically-bound sulphur in high-molecular-weight sedimentary organic matter using flash pyrolysis and Raney Ni desulfurisation. *In* W. L. Orr and C. M. White (eds). *Geochemistry of Sulfur in Fossil Fuels.* ACS symposium series, **429**, 486-528.

SINNINGHE-DAMSTÉ, J. S., EGLINTON, T. I., DE LEEUW, J. W. and SCHENCK, P. 1989. Organic sulphur in macromolecular sedimentary organic matter: I. Structure and origin of sulphur-containing moieties in kerogen, asphaltenes and coal as revealed by flash pyrolysis. *Geochimica et Cosmochimica Acta*, **53** (4), 873-889.

SINNINGHE-DAMSTÉ, J. S., IRENE, W., RIJPSTRA, C., DE LEEUW, J. W. and SCHENCK, P. 1988. Origin of organic sulphur compounds and sulphur-containing high molecular weight substances in sediments and immature crude oils. *Organic Geochemistry*, **13** (4-6), 593-606.

SLATER, T. S., MCNAMARA, M. E., ORR, P. J., FOLEY, T. B., ITO, S. and WAKAMATSU, K. 2020. Taphonomic experiments resolve controls on the preservation of melanosomes and keratinous tissues in feathers. *Palaeontology*, **63** (1), 103-115.STANKIEWICZ, B., BRIGGS, D. E. G., MICHELS, R., COLLINSON, M., FLANNERY, M. and EVERSHED, R. 2000. Alternative origin of aliphatic polymer in kerogen. *Geology*, **28** (6), 559-562.

STANKIEWICZ, B., SCOTT, A., COLLINSON, M. E., FINCH, P., MÖSLE, B., BRIGGS, D. and EVERSHED, R. 1998. Molecular taphonomy of arthropod and plant cuticles from the Carboniferous of North America: implications for the origin of kerogen. *Journal of the Geological Society*, **155** (3), 453-462.

STAROŃ, P., BANACH, M. and KOWALSKI, Z. 2011. Keratyna: źródła, właściwości, zastosowanie. *Chemik*, **65** (10), 1019-1026.

STĘPIEŃ, K., DZIERŻĘGA-LĘCZNAR, A., KURKIEWICZ, S. and TAM, I. 2009. Melanin from epidermal human melanocytes: study by pyrolytic GC/MS. *Journal of the American Society for Mass Spectrometry*, **20** (3), 464-468

933 SULLIVAN, C., WANG, Y., HONE, D. W., WANG, Y., XU, X. and ZHANG, F. 2014. The vertebrates
934 of the Jurassic Daohugou Biota of northeastern China. *Journal of Vertebrate Paleontology*, **34**
935 (2), 243-280.
936 TEGELAAR, E. W., DE LEEUW, J. W., DERENNE, S. and LARGEAU, C. 1989. A reappraisal of
937 kerogen formation. *Geochimica et Cosmochimica Acta*, **53** (11), 3103-3106.
938 TEMPLIER, J., GALLOIS, N. and DERENNE, S. 2013. Analytical TMAH pyrolysis of dipeptides:
939 Formation of new complex cyclic compounds related to the presence of the peptide bond.
940 *Journal of Analytical and Applied Pyrolysis*, **104**, 684-694.
941 WANG, Y. X. and CAO, X. J. 2012. Extracting keratin from chicken feathers by using a hydrophobic
942 ionic liquid. *Process Biochemistry*, **47**, 896-899.
943 WANG, B., ZHAO, F., ZHANG, H., FANG, Y. and ZHENG, D. 2012. Widespread pyritization of
944 insects in the Early Cretaceous Jehol Biota. *Palaios*, **27** (10), 708-712.
945 WIEMANN, J., FABBRI, M., YANG, T. R., STEIN, K., SANDER, P. M., NORELL, M. A. and
946 BRIGGS, D. E. 2018. Fossilization transforms vertebrate hard tissue proteins into N-heterocyclic
947 polymers. *Nature communications*, **9** (1), 4741.
948 WILBY, P. R., BRIGGS, D. E. G. and RIOU, B. 1996. Mineralization of soft-bodied invertebrates in a
949 Jurassic metalliferous deposit. *Geology*, **24** (9), 847-850.
950 WOGELIUS, R., MANNING, P., BARDEN, H., EDWARDS, N., WEBB, S., SELLERS, W.,
951 TAYLOR, K., LARSON, P., DODSON, P. and YOU, H. 2011. Trace metals as biomarkers for
952 eumelanin pigment in the fossil record. *Science*, **333** (6049), 1622-1626.
953 WOJCIECHOWSKA, E., ROM, M., WŁOCHOWICZ, A., WYSOCKI, M. and WESEŁUCHA-
954 BIRCZYŃSKA, A. 2004. The use of Fourier transform-infrared (FTIR) and Raman spectroscopy

(FTR) for the investigation of structural changes in wool fibre keratin after enzymatic treatment. *Journal of Molecular Structure*, **704** (1-3), 315-321.

XING, L., MCKELLAR, R. C., XU, X., LI, G., BAI, M., PERSONS, W.S., MIYASHITA, T., BENTON, M. J., ZHANG, J. and WOLFE, A. P. 2016. A feathered dinosaur tail with primitive plumage trapped in Mid-Cretaceous amber. *Current Biology*, **26** (24), 3352-3360.

XU, X., WANG, ZHANG, K., MA, Q., XING, L., SULLIVAN, C., HU, D., CHENG, S. and WANG, S. 2012. A gigantic feathered dinosaur from the Lower Cretaceous of China. *Nature*, **484** (7392), 92-95.

XU, X., WANG, X. L. and WU, X. C. 1999. A dromaeosaurid dinosaur with a filamentous integument from the Yixian Formation of China. *Nature*, **401** (6750), 262-266.

XU, X., ZHAO, Q., NORELL, M., SULLIVAN, C., HONE, D., ERICKSON, G., WANG, X. L., HAN, F. L. and GUO, Y. 2009. A new feathered maniraptoran dinosaur fossil that fills a morphological gap in avian origin. *Chinese Science Bulletin*, **54** (3), 430-435.

XU, X., ZHENG, X., SULLIVAN, C., WANG, X., XING, L., WANG, Y. X., ZHANG, X., O'CONNOR, J. K., ZHANG, F. and PAN, Y. 2015. A bizarre Jurassic maniraptoran theropod with preserved evidence of membranous wings. *Nature*, **521** (7550), 70-73.

YANG, J. H., WU, F. Y., SHAO, J. A., WILDE, S. A., XIE, L. W. and LIU, X. M. 2006. Constraints on the timing of uplift of the Yanshan Fold and Thrust Belt, North China. *Earth and Planetary Science Letters*, **246**, 336-352.

YOSHIMIZU, H. and ANDO, I. 1990. Conformational characterization of wool keratin and 5'-(Carboxymethy1) kerateine in the solid state by ^{13}C CP/MAS NMR spectroscopy. *Macromolecules*, **23**, 2908-2912.

YUAN, H., LIU, X., LIU, Y., GAO, S. and LING, W. 2005. Geochemistry and U-Pb zircon geochronology of Late-Mesozoic lavas from Xishan, Beijing. *Science in China: Series D Earth Sciences*, **49** (1), 50-67.

YU, P., MCKINNON, J. J., CHRISTENSEN, C. R. and CHRISTENSEN, D. A. 2004. Using synchrotron-based FTIR microspectroscopy to reveal chemical features of feather protein secondary structure: comparison with other feed protein sources. *Journal of agricultural and food chemistry*, **52** (24), 7353-7361.

ZHANG, H., WANG, M. X. and LIU, X. M. 2008. Constraints on the upper boundary age of the Tiaojishan Formation volcanic rocks in West-Liaoning –North Hebei by LA-ICP-MS dating. *Chinese Science Bulletin*, **53** (22), 3574-3584.

ZHAO, T., HU, J., HU, L. and PAN, Y., 2020. Experimental maturation of feathers: implications for interpretations of fossil feathers. *Palaios*, **35** (2), 67-76.

ZHENG, X. T., YOU, H. L., XU, X. and DONG, Z. M. 2009. An early Cretaceous heterodontosaurid dinosaur with filamentous integumentary structures. *Nature*, **458**, 333-336.

ZHOU, Z., JIN, F. and WANG, Y. 2010. Vertebrate assemblages from the Middle-Late Jurassic Yanliao Biota in northeast China. *Earth Science Frontier*s, **17**, 252-254.

ZHU, M., BABCOCK, L. E. and STEINER, M. 2005. Fossilization modes in the Chengjiang Lagerstätte (Cambrian of China): testing the roles of organic preservation and diagenetic alteration in exceptional preservation. *Palaeogeography, Palaeoclimatology, Palaeoecology*, **220**, 31-46.

FIGURE CAPTIONS

998 Figure 1. *Anchiornis huxleyi* (YFGP-T5199). Photograph of the Jurassic feathered theropod with
999 location of sampled areas. The white box indicates locations of fossil feather and 'host' sediment
1000 sampling, while the yellow box indicates location of 'remote' sediment sampling, for NMR, Py-GC-MS,
1001 and IBA analyses. White dots are samples used for SEM imaging and EDS. Scale bar = 5 cm.
1002 Photograph by Thierry Hubin (IRSNB).

1003 Figure 2. Scanning electron microscopy (SEM) images of minerals observed in the plumage of
1004 *Anchiornis huxleyi*. (A), (B) thin platelets of phyllosilicates observed in sample 7 (see Fig. 1 for
1005 location); scale bar = 5 µm (A) and 3 µm (B), (C) Pyrite framboids (sample 1); scale bar = 10 µm, (D)
1006 Pyrite crystallites (sample 1); scale bar = 5 µm, (E) Clayed pores containing small star-shaped iron-
1007 oxide crystals (sample 8); scale bar = 2 µm, (F) Star-shaped iron oxides (sample 1); scale bar = 2 µm,
1008 (G) Feldspar crystal surrounded by clay sheets (sample 5); scale bar = 5 µm, (H) Quartz crystals
1009 embedded in a clayed matrix (sample 9); scale bar = 5 µm. Arrowheads point towards the
1010 aforementioned minerals. Abbreviations: Phy: phyllosilicate; Py: pyrite; Fd: feldspar; Qz: quartz.

1011 Figure 3. X-ray powder diffraction patterns of the 'host' sediment. Spectrum of (A) the bulk rock; qz,
1012 quartz; ca, calcite, (B) the fraction < 2 µm, with spectra of natural (N), glycolated (G), and heated (H)
1013 sample. The expansive illite/smectite interstratifications are identified in the spectrum of the glycolated
1014 (G) material.

1015 Figure 4. SEM images of the ultrastructure of *Anchiornis* plumage. (A), (B) elongated microbodies
1016 observed in sample 6 (see Fig. 1 for location), (C) Elongated microbodies (arrows) observed in sample
1017 9, and (D) imprints observed in samples 6. Scale bars: 2 µm.

1018 Figure 5. Results of Elastic Backscattering Spectrometry (EBS) and Particle-Induced X-ray Emission
1019 (PIXE) analyses on the fossil feathers, the 'host' sediment and the 'remote' sediment. (A) Global content
1020 of C, O and Si obtained by EBS, in integrating the C, O and Si depth profiles over the 0 – 25 000 TFU
1021 interval. The error bars give an estimate of the uncertainties considering the counting statistics as well as
1022 the cross-section and stopping power uncertainties. Analysis have been performed in duplicate on the
1023 same area of the fossil feather (Fossil #1, Fossil #2), three points of analysis have been taken at three
1024 different locations in the 'host' sediment (at 1.7, 3.2, and 4.8 mm away from the fossil), and one in the
1025 remote sediment (B) PIXE spectra obtained for one point of analysis in the fossil feather (red), the 'host'
1026 sediment (black), and the remote sediment (blue). The spectra are normalized to the Al signal (which is
1027 mainly coming from the selective filter) to allow for a direct comparison.

1028 Figure 6. Cross polarization/magic angle spinning ^{13}C nuclear magnetic resonance (CP-MAS ^{13}C-NMR)
1029 spectra of (A) the modern bird feather, (B) the fossil feathers, and (C) the 'host' sediment. Major
1030 chemical functions are indicated on each peak.

1031 Figure 7. IR spectra showing the comparison between of (A) a modern buzzard feather and *Anchiornis*
1032 feathers, and (B) *Anchiornis* feathers and the sedimentary matrix ('remote' sediment). See the text for
1033 peak assignment. The spectra are normalized to 100 % transmittance.

1034 Figure 8. Chromatograms of the products formed during the pyrolysis of (A) modern buzzard feathers,
1035 (B) fossil feathers, and (C) remote sediment. Peak identifications are given in Tables 2 and 3. C_n: carbon
1036 chain, with *n* indicating the length of the chain.

1037 Table 1. Sulphur content derived from PIXE using GUPIX for the data reduction. The global uncertainty
1038 is obtained by combining the counting statistics and the fit error (both calculated by GUPIX) with the

1039 estimated accuracy of our PIXE measurements. The latest contribution is obtained by direct comparison
1040 to a BCR-126A certified reference material. The global uncertainty is obtained by summing these three
1041 contributions in quadrature.

1042 Table 2. Significance of the peaks observed on the pyrochromatogram of the modern bird feather. Peaks
1043 are listed by increasing retention times. The table shows the complete name of each identified
1044 compound, the origin of these compounds, and whether they are observed in the modern feather, the
1045 fossil plumage, and the sediment. Peaks 1-18 and a-e were observed in the spectrum of the modern
1046 feathers, peaks f-g were observed in the spectrum of the fossil feather.

1047

Appendix

Molecular structures of compounds identified in the modern bird feathers. The correspondence with the numbers appears in Table 2 and Figure 8.

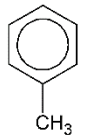

1

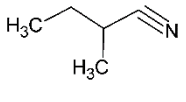

2

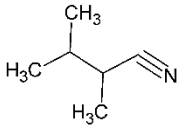

3

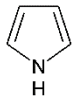

4

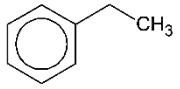

5

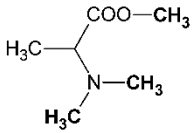

6

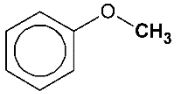

7

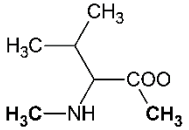

8

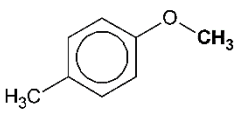

9

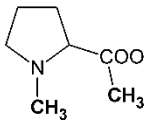

10

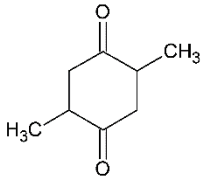

11

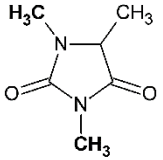

12

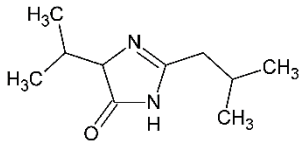

13

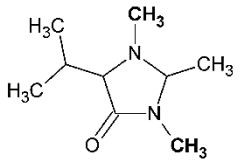

14

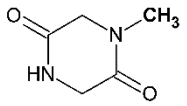

15

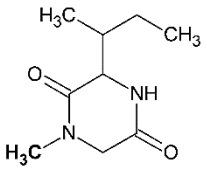

18

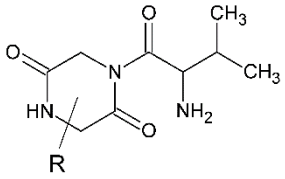

19

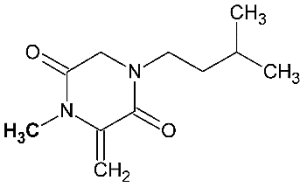

20,21

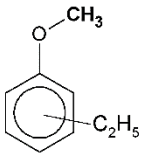

22

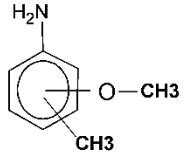

23

1077

1078

1079

1080

1081

1082

1083

1084

1085

1086

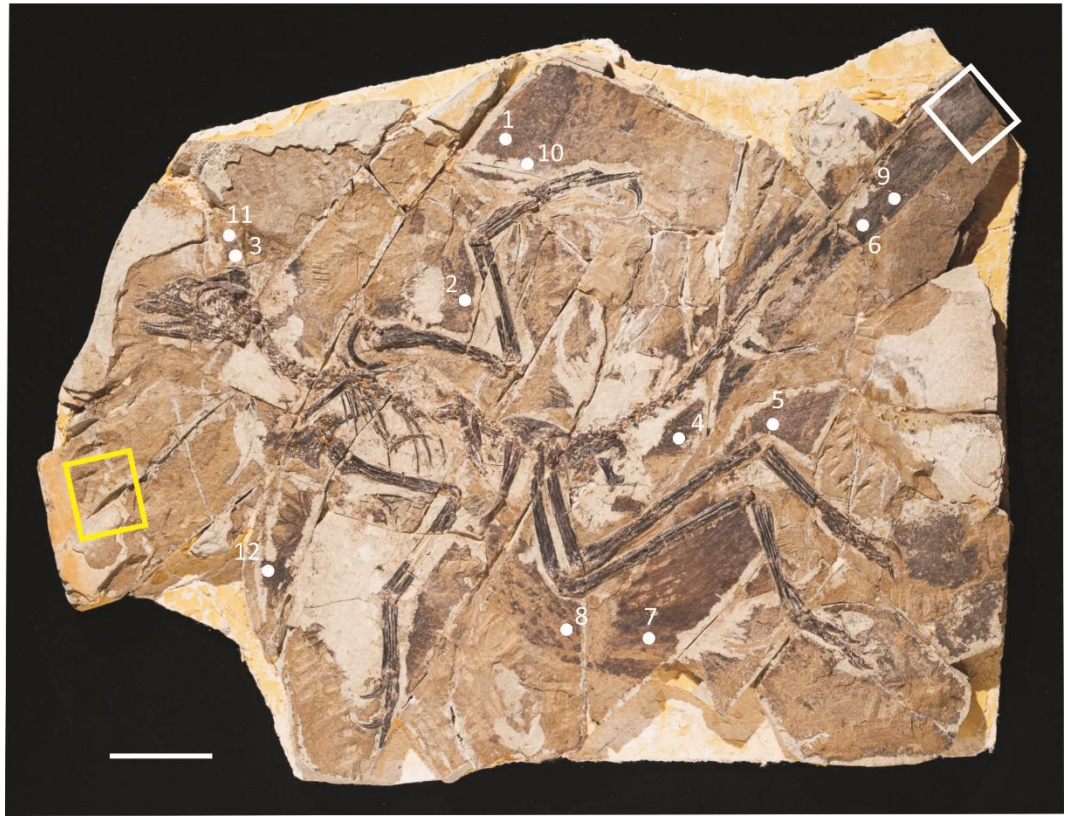

1087

1088

1089

1090

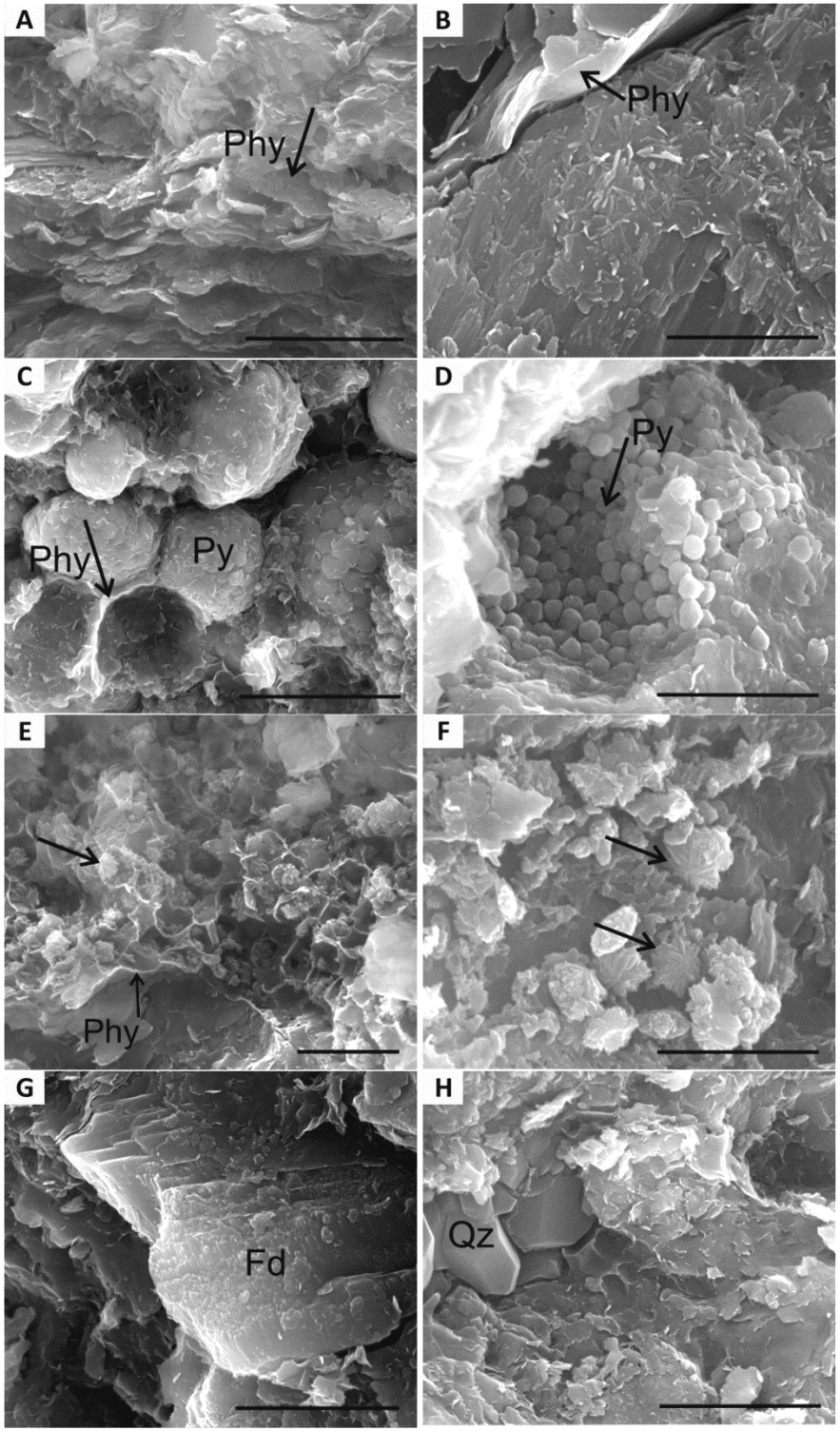

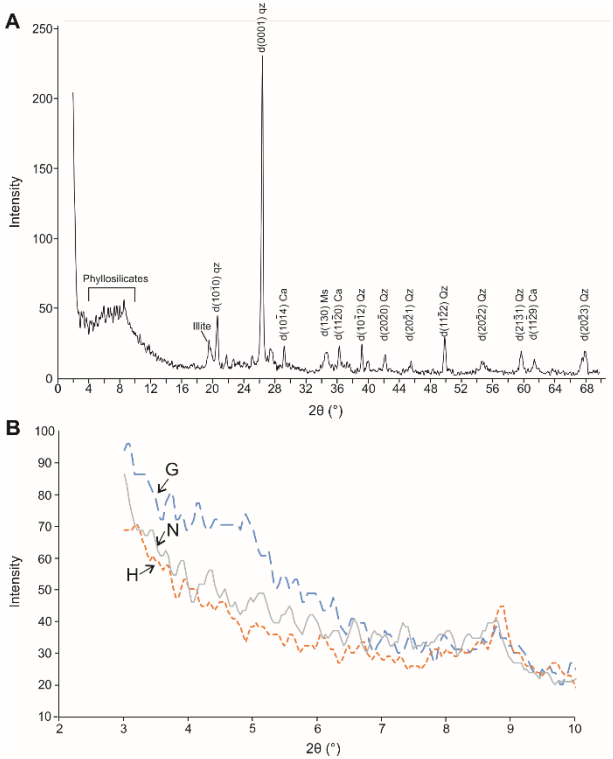
A
Intensity
Phyllosilicates
Illite
d(0001) qz
d(10$\bar{1}$4) Ca
d(1120) Ms
d(1120) Ca
d(10$\bar{1}$2) Qz
d(20$\bar{2}$0) Qz
d(20$\bar{2}$1) Qz
d(11$\bar{2}$2) Qz
d(20$\bar{2}$2) Qz
d(2$\bar{1}$31) Qz
d(1129) Ca
d(20$\bar{2}$3) Qz
2θ (°)
B
Intensity
G
N
H
2θ (°)

1091

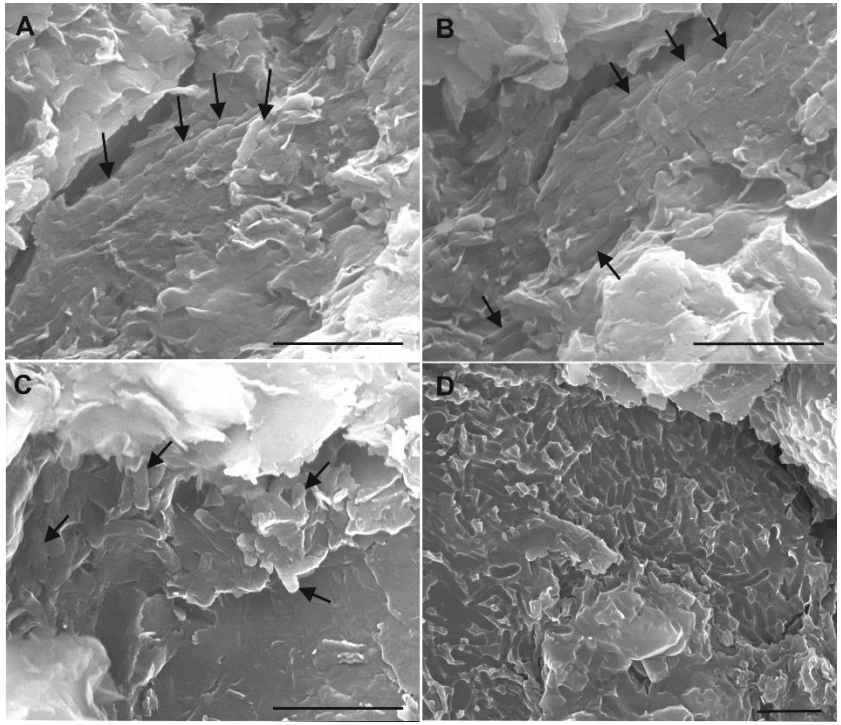

1092

1093

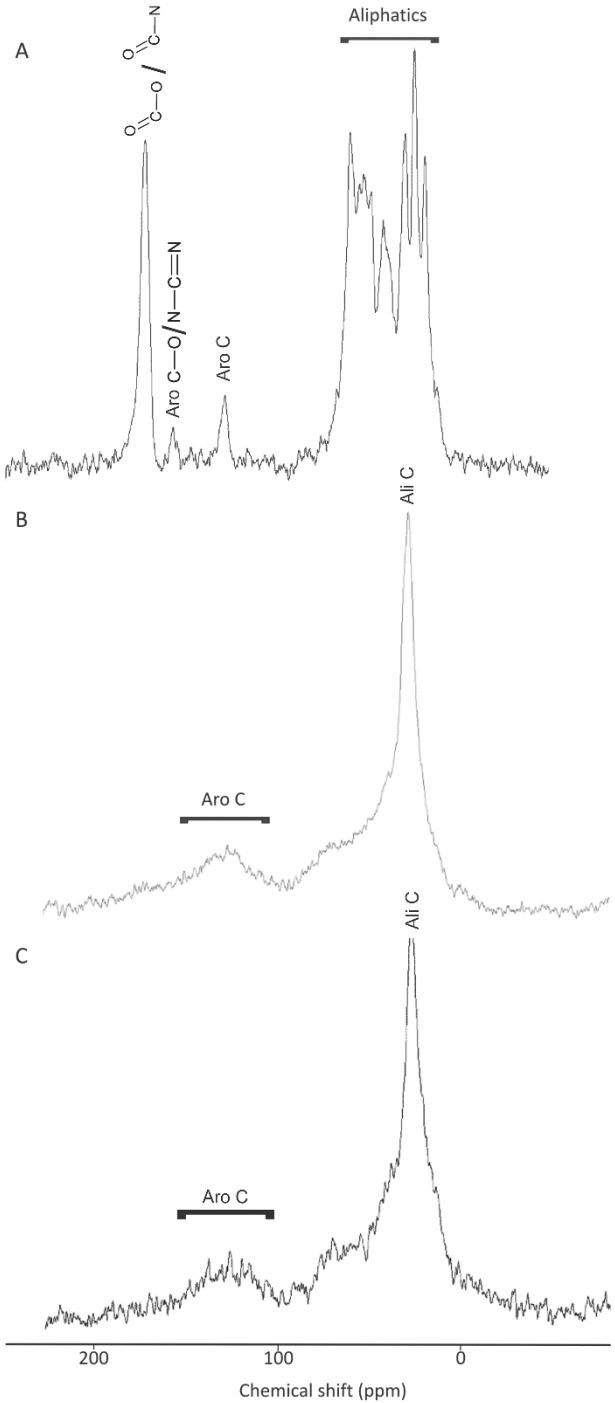
A
Aliphatics
Aro C
Aro C
B
Ali C
Aro C
C
Ali C
Aro C
200
100
0
Chemical shift (ppm)

58

1094

1095

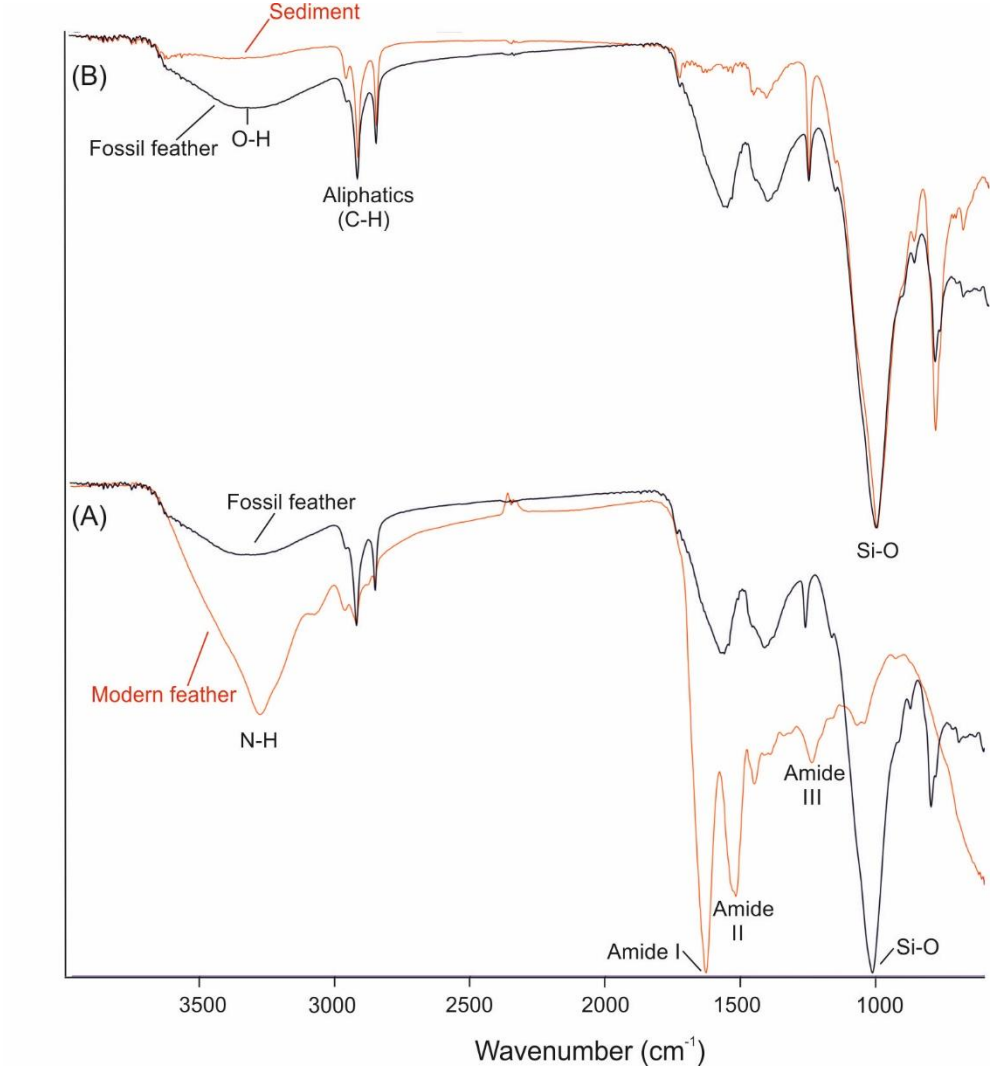
Sediment
(B)
Fossil feather
O-H
Aliphatics
(C-H)
Si-O
(A)
Fossil feather
Modern feather
N-H
Amide
III
Amide
II
Amide I
Si-O
3500
3000
2500
2000
1500
1000
Wavenumber (cm-1)

1096

1097

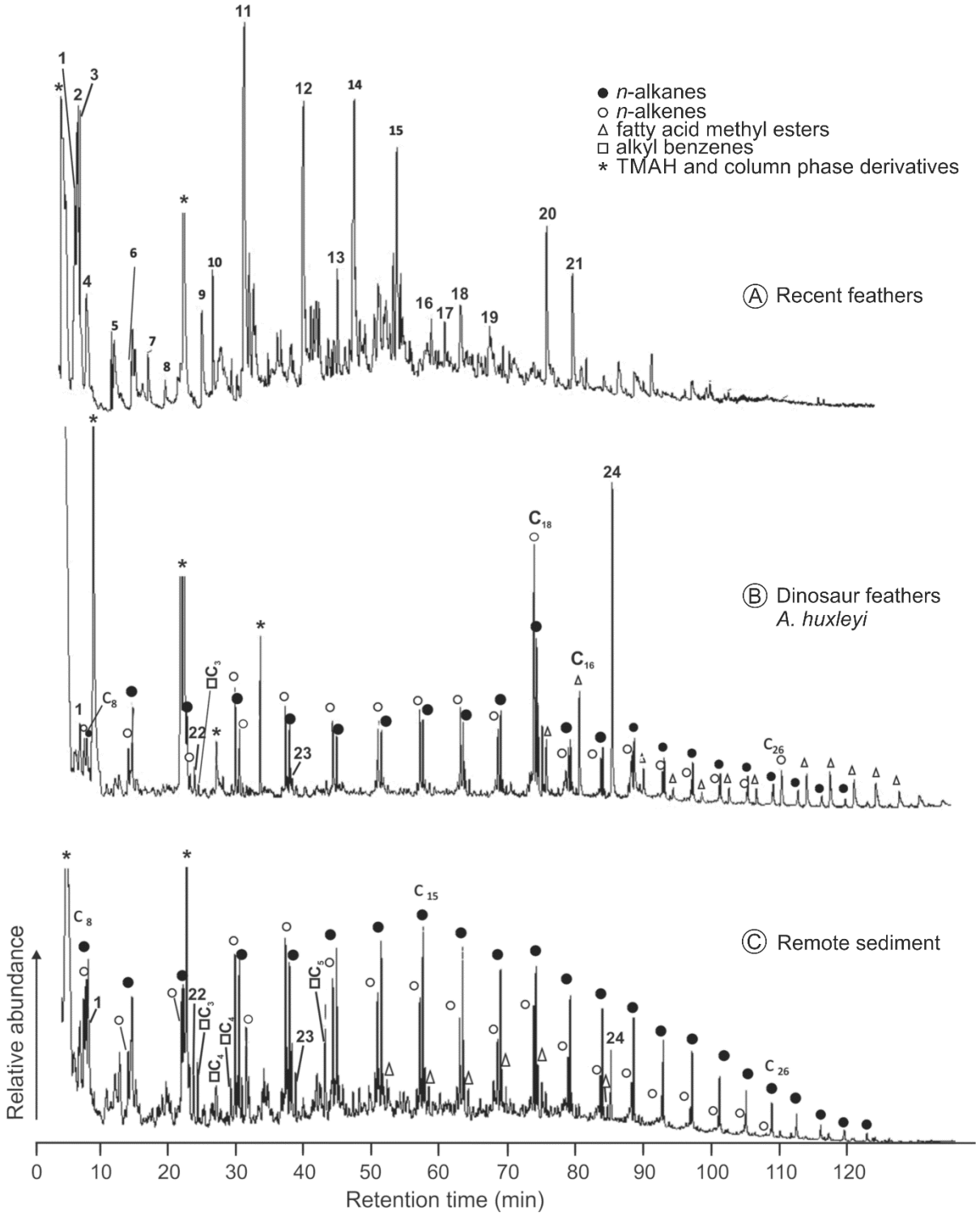
● n-alkanes
○ n-alkenes
△ fatty acid methyl esters
□ alkyl benzenes
* TMAH and column phase derivatives
Ⓐ Recent feathers
Ⓑ Dinosaur feathers
A. huxleyi
Ⓒ Remote sediment
Relative abundance
Retention time (min)
0 10 20 30 40 50 60 70 80 90 100 110 120

Table 1. PIXE derived concentration data for S and C in the fossil and modern feathers, and "host" sediment. The numbers in the left row represent the distance of the analyzed spots, away from the feather/sediment boundary. See Supplementary Table 1 for details on the global uncertainty calculations, Figure 1 and Supplementary Figure 2 for the location of the analyses.

	[S] (ppm)	[C] (ppm)
Fossil Feather #1	1739	80,385
Fossil Feather #2	1946	82,171
+1.7 mm	1162	72,012
+3.2 mm	801	49,213
+4.8 mm	893	41,835
Remote sediment	98	20,331
Rachis	37,142	547,174
Barbs	43,070	314,962

1101

Peak	Retention time (min)	Major characteristic ions[a] (m/z)	Molecular ion	Compound	Possible origin[b]	Modern feather	Fossil feather[c]	Embedding sediment[c]
1	6.7	91; 92; 39; 65	92	Methylbenzene	(Phe)	X	X	X
2	6.9	55, 54, 42	83	2-methylbutanenitrile	Ileu	X		
3	7,1	43, 41, 39, 68	83	3-methylbutanenitrile	Leu	X		
4	8.0	67; 41; 39; 40	67	1*H*-Pyrrole	(Ser)	X		
5	12.1	91; 55; 106; 65	106	Ethylbenzene	(Phe)	X		
6	14.8	72; 42; 56; 131	131	N,N- Dimethylalanine methylester	Ala	X		
7	17.0	108; 78; 65; 39	108	Methoxybenzene	Tyr	X		
8	19.5	86; 102; 42; 55	145	N-Methyl-valine Methyl Ester	Val	X		
9	25.0	122; 77; 107; 91	122	1-Methoxy-4-methylbenzene	Tyr	X		
10	26.5	84; 42; 100; 58	143	N-Methyl-proline Methyl Ester	Pro	X		
11	31.2	56; 140; 42; 112; 83	140	2,5-Dimethylcyclohexane-1,4-Dione	Gly	X		
12	39.7	42; 127; 142; 56	142	1,3,5-Trimethylimidazolidine-2,4-Dione	Ala?	X		
13	44.8	56; 126; 139; 41	182	1-Isobutyl-4-isopropylimidazolinone	Val	X		
14	47.2	128; 42; 71; 113	170	5-Isopropyl-1,2,3-trimethylimidazolidinone	Val-(Gly)	X		
15	53.6	128; 42; 57; 71	128	1-Methylpiperazine-2,5-dione	Gly	X		
16	58.6	82; 167; 182; 110	182	?	His?	X		
17	60.5	152; 41; 55; 137; 179	194	?	Val?	X		
18	62.9	142; 113; 42; 71	198	1-Methyl-3-(1-methylpropyl)piperazine-2,5-dione	Ileu-Gly	X		
19	67.1	142; 113; 42; 98; 212	?	N-(1-oxo-2-amino-3-methyl-butyl)piperazine-2,5-dione derivative	Val	X		
20	75.5	139; 70; 42; 168	210	N-Methyl-3-methylidene-6-(3-methylbutyl)piperazine-2,5-dione	Ser-Leu	X		
21	79.2	168; 139; 70; 42	210	Isomer of compound 20	Ser-Leu	X		
22	23.7	136, 121, 122, 91	136	1-Methoxy-2,3-dimethylbenzene or 1-Ethyl-2-methoxybenzene	Lignin or cellulose		X	X
23	38.1	136, 122, 137	137	Methoxy-methylaniline	?		X	X
24	86.3	45; 57; 97; 224; 252	284	1-Methoxyoctadecane	?		X	X
●		43; 57; 71; 85		*n*-alkanes	Aliphatic chains		C_8-C_{30} (C_{18}, C_{11})	C_8-C_{29} (C_{15})
○		55; 43; 69; 83, 97		*n*-alk-1-enes	Aliphatic chains		C_8-C_{26} (C_{11}, C_{18})	C_8-C_{29} (C_{11}, C_{18})
Δ		87; 74; 43; 55		Fatty acid methyl esters	Aliphatic chains		C_8-C_{30} (C_{16})	C_8-C_{30} (C_{16})
□		91, 105		Alkyl benzenes	?		C_3	C_3-C_5 (C_5)

Table 2. Main products released from pyrolysis of modern feathers, fossil feathers and embedding sediment in the presence of TMAH.

[a] MS fragments are in order of decreasing abundance, with base peak underlined.

[b] Compounds in brackets indicate possible origin that is not univocal; Ala, alanine; Gly, glycine; His, histidine; Phe, phenylalanine; Pro, proline; Ser, serine; Tyr, tyrosine; Val, valine; ? Tentative origin

[c] C_{range} (C_{max}, C_{submax})